The
ENGINEERS DIGEST

REVIEW OF ENGINEERING PROGRESS ABROAD

VOL. IX. No. 3 MARCH, 1948

ENGINEERING LIBRARY
APR 1 1948

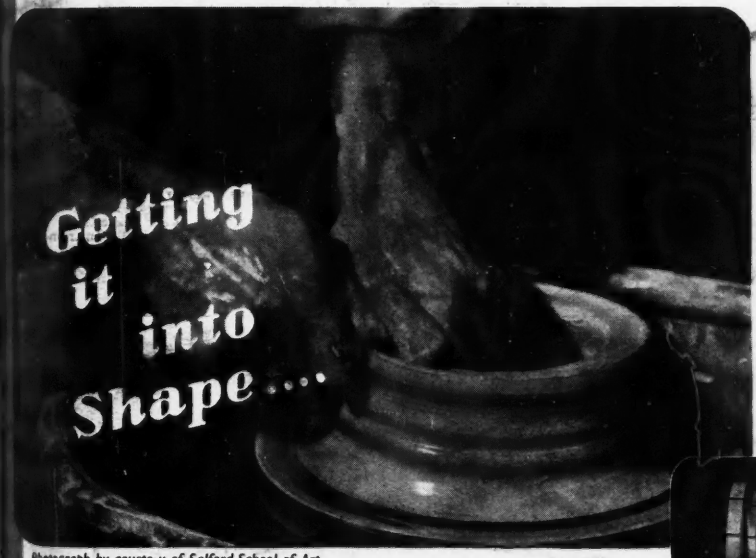

1. Steering Worm.
2. Acme Thread.
3 & 4. Ball Thread.
5. Special Acme Thread.
6. Valve Seat Inserts.
7. Reduction Gear Tooth Form.
8. "Jet" Propulsion Blade Root.

Photograph by courtesy of Salford School of Art.

.... is not as easy as it looks. Many years of experience are required before a "technique" can be evolved—and this same experience—40 years to be exact—is responsible for the perfection of Form Grinding on Churchill Precision Machines, using

"The PULCRUSH"

method—the greatest advance yet made in wheel forming. The forms illustrated are a few of the countless contours that can be transferred to the grinding wheel of all machines on which the periphery of the wheel is used.

Our Technical Department is able to give advice on all wheel forming queries.

The
CHURCHILL MACHINE TOOL Co. Ltd.
BROADHEATH MANCHESTER

THE ENGINEERS' DIGEST

Published Monthly by Engineers' Digest Ltd., 120 Wigmore Street, London, W.1. Tel.: WELBECK 9357

ANNUAL SUBSCRIPTION OF 12 NUMBERS, £2 2s. :: **SINGLE COPIES, 4s. 6d.**

ADVISORY COMMITTEE

J. F. ALCOCK, B.A., M.I.Mech.E.
R. W. ALLOTT, M.A., A.R.Ae.S.
E. ALTON, D.Eng., A.M.Inst.B.E.
R. W. AYERS, M.I.W.
Col. J. BOWDEN, M.Inst.C.E., M.I.Mech.E.
H. H. BROUGHTON, M.I.Mech.E.
F. BUCKINGHAM, B.Sc., A.M.Inst.C.E., A.M.I.Mech.E., A.M.I.E.E.
T. H. BURNHAM, B.Sc. (Lond.), A.M.I.Mech.E.
J. S. CASWELL, M.Sc., M.I.Mech.E.
G. C. SAFFERY COOPER.
J. DICK, Ph.D., B.Sc., A.M.I.Mech.E.
D. FIFE, M.I.Mech.E.
G. E. FOXWELL, D.Sc. (Lond.), F.Inst.P. F.Inst.F., M.Inst.Gas.E.
R. GRIFFITHS, M.Sc.
H. HEYWOOD, D.Sc., Ph.D., M.I.Mech.E.
O. HURST, M.Inst.N.A.
Capt. J. S. IRVING, M.I.Mech.E., M.I.A.E., A.F.R.Ae.S., M.S A.E.
F. C. JOHANSEN, M.Sc. (Eng.), M.I.Mech.E., F.R.Ae.S., M.I.Loco.E.
W. J. KEARTON, D.Eng., M.I.Mech.E., A.M.Inst.N.A.
Prof. W. KERR, Ph.D., M.I.Mech.E.
G. V. LOMONOSOFF, Dr.Ing., M.I.Mech.E.
B. J. LYMER, M.I.Mech.E.
D. T. MACIVOR, M.I.Mech.E., M.Cons.E.
W. O. MANNING, F.R.Ae.S.
R. B. MATTHEWS, Wh.Ex., A.M.Inst.C.E., M.I.E.E., F.R.Ae.S.
Prof. A. L. MELLANBY, D.Sc., LL.D., M.I.Mech.E.
J. H. R. RATCLIFFE, B.Sc. (Eng., Hons.), M.I.Mech.E.
Col. C. W. D. ROWE.
W. A. SCOBLE, D.Sc., A.R.C.Sc., M.I.Mech.E.
P. W. SEEWER, D.E. (Zurich), M.Int.C.E., M.I.Mech.E.
Prof. S. PARKER SMITH, D.Sc., M.I.E.E., A.M.Inst.C.E.
C. E. H. VERITY, A.M.Inst.C.F., A.M.I.E.E., A.M.I.Mech.E.
E. G. WALKER, F.C.G.I., B.Sc. (Eng.), M.Inst.C.E., M.I.Mech.E., M.A.Soc.C.E.
Major F. L. WATSON, M.I.C.E., M.I.Mech.E.
G. WATSON, M.Inst.C.E., M.I.Mech.E.
R. J. McL. WHIBLEY, A.M.I.Mech.E.
C. H. WOODFIELD, M.I.Mech.E., M.I.Struct.E.
T. WRIGHT, Ph.D., M.Sc.
M. L. YATES, Ph.D., M.Sc.Tech., M.A. (Com.) M.I.Mech.E.

ADVISORY COMMITTEE OF THE AMERICAN EDITION

Chairman: DR. ALEXANDER KLEMIN, New York University.

R. S. ARCHER, Climax Molybdenum Company.
Prof. O. W. BOSTON, University of Michigan.
Dr. W. H. CARRIER, Carrier Corporation.
R. W. CARSON, Instrument Specialties Co., Inc.
Dr. L. W. CHUBB, Westinghouse Electric Corp.
A. E. RICHARD DE JONGE, Babcock & Wilcox Co.
Dr. O. S. DUFFENDACK, North American Phillips Co.
HANS ERNST, Cincinnati Milling Machine Co.
R. D. EVANS, The Goodyear Tire & Rubber Co.
CHRISTIAN E. GROSSER, Standard Machinery Co.
GEORGE F. HABACH, Worthington Pump & Machinery Corp.
Dr. VICTOR O. HOMERBERG, The Nitralloy Corp.
HERBERT R. ISENBURGER, St. John X-ray Service.
J. B. JOHNSON, A.A.F., Wright Field.
CHARLES M. JONES, John A. Roebling's Sons Co.
H. MANDEL The Wickman Corp.
J. C. MATHES, Dow Chemical Co.
H. W. MCQUAID, Republic Steel Corp.
R. F. MILLER, Carnegie-Illinois Steel Corp.
Professor L. F. MOODY, Princeton University.
Professor H. F. MOORE, University of Illinois.
LAWRENCE OTTINGER, United States Plywood Corp.
C. E. PRITCHARD, Republic Steel Corp.
JOHN SANDS, International Nickel Co.
JAMES G. SAWYER, Buffalo Turbine Corp.
Dr. A. O. SCHMIDT, Kearney & Trecker Corp.
L. K. SILLCOX, New York Air Brake Co.
ALBERT F. SPERRY, President, Instrument Society of America.
R. DAVID THOMAS, JR., Arcos Corp.
GEORGE A. TINNERMAN, Tinnerman Products, Inc.

CONTENTS

	Page
Apparatus for the Rapid Taking of Magnetization Curves "*The Engineers' Digest*," Vol. 9, No. 3, *p.* 85.	85
The Calculation of the most favourable Working Conditions for Chip Producing Machining Operations "*The Engineers' Digest*," Vol. 9, No. 3, *p.* 75.	75
Classified Abstracts "*The Engineers' Digest*," Vol. 9, No. 3, *p.* 101.	101
Dimensioning Permanent Magnets "*The Engineers' Digest*," Vol. 9, No. 3, *p.* 91.	91
The Effect of Shape and Size Factors on Fatigue Strength "*The Engineers' Digest*," Vol. 9, No. 3, *p.* 96.	96
Electrical Drives Without Reduction Gearing "*The Engineers' Digest*," Vol. 9, No. 3, *p.* 80.	80
An Electric Flow Meter "*The Engineers' Digest*," Vol. 9, No. 3, *p.* 73.	73
Fractographic Studies of Ferro-Chromium Alloys "*The Engineers' Digest*," Vol. 9, No. 3, *p.* 87.	87
News of the Month "*The Engineers' Digest*," Vol. 9, No. 3, *p.* 103.	102
Volvo Diesel Series "*The Engineers' Digest*," Vol. 9, No. 3, *p.* 71.	71
The Use of the Expansion of Gases in a Centrifugal Field "*The Engineers' Digest*," Vol. 9, No. 3, *p.* 82.	82

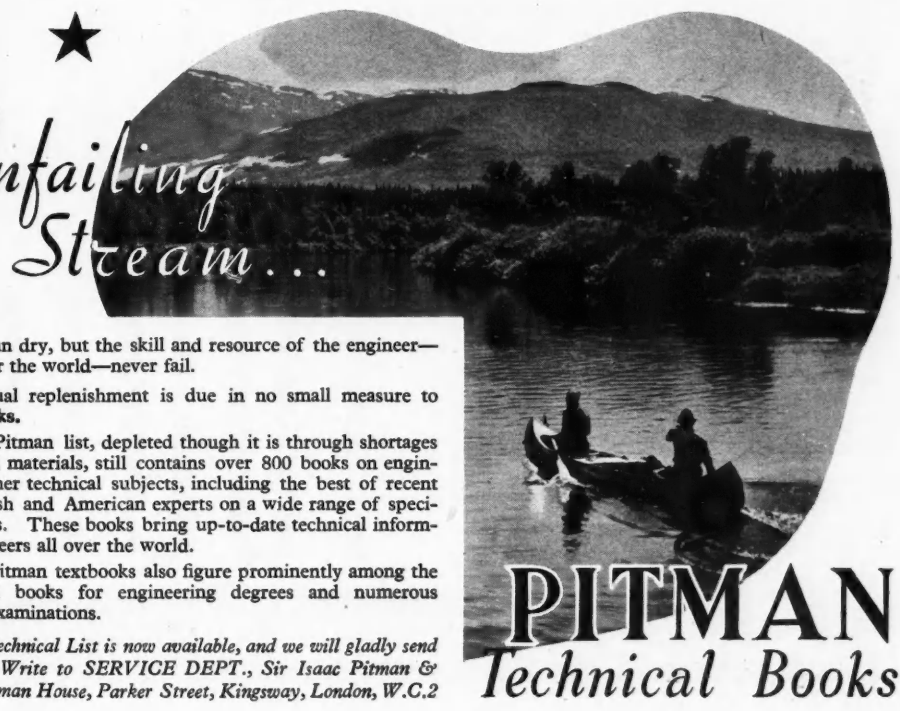

Rivers may run dry, but the skill and resource of the engineer—fortunately for the world—never fail.

Their continual replenishment is due in no small measure to **Pitman Books.**

The current Pitman list, depleted though it is through shortages of labour and materials, still contains over 800 books on engineering and other technical subjects, including the best of recent work by British and American experts on a wide range of specialized subjects. These books bring up-to-date technical information to engineers all over the world.

Established Pitman textbooks also figure prominently among the recommended books for engineering degrees and numerous professional examinations.

Our revised Technical List is now available, and we will gladly send you a copy. Write to SERVICE DEPT., Sir Isaac Pitman & Sons Ltd., Pitman House, Parker Street, Kingsway, London, W.C.2

PITMAN
Technical Books

Butt Welded TOOLS

ENGLISH STEEL CORPORATION LTD OPENSHAW MANCHESTER

Volvo Diesel Series

By J. STALBLAD. (From *Teknisk Tidskrift*, Vol. 77, No. 46, 1947, pp. 849-853. 14 illustrations.)

THE development of Volvo Diesels for buses and lorries was taken in hand shortly after the outbreak of World War II, and by 1941 a number of experimental 6·13 litre engines was ready for testing. These experimental engines were first built for direct injection and with the combustion space placed mainly within the piston crown. Special tests were carried out to investigate the effects of the division of the combustion space into a space contained within the piston crown and another space represented by the cylinder space proper. These tests also included a study of the influence of the ratio of piston combustion space/total combustion space, upon engine economy.

In the first experimental engine the piston combustion space approximated to 66 per cent of the total combustion space, that is to say, the combustion space in the cylinder proper amounted to 34 per cent of the total volume. By placing both inlet and exhaust valve in the cylinder head, the combustion space in the piston crown was increased to 86 per cent ; this alteration caused an increase in the compression ratio from 16 to 18 and the resulting improvement in fuel economy was found to be considerable, as evidenced by Fig. 1 ; in fact, it is greater than would be expected as a result of the increase in compression ratio effected.

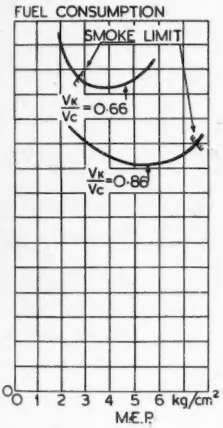

Fig. 1. **Fuel consumption as a function of m.e.p.**
v_k = Volume of combustion cavity in piston.
v_c = Total combustion space.

The running characteristics of the experimental engine indicated the need for making provision for adjustibility of the advance angle of injection. This need was emphasized by the relatively poor fuel economy and the low smoke limit obtained with constant advance angle. It will be seen from Fig. 2 that for curve *A* the smoke limit of an engine operating with manually-controlled advance angle is so adjusted that the engine always shows optimum fuel economy for the fuel pump stroke and load considered. In order to examine the advantages of automatically acting advance angle control, the engine was then operated with constant advance angle, and from curve *B* it will be noted that a considerably more favourable smoke limit obtains with manually-adjusted advance angle. This test therefore furnished proof that the advance angle should be varied with the engine speed.

The investigation of the combustion process in the cylinder was carried out by means of a multiple indicator ; a typical pressure-time card is reproduced in Fig. 3. The indicator diagrams were taken at an engine speed of 1,000 r.p.m., the m.e.p. being 6·18 kg. per sq. cm. It was soon found, however, that this indicator was not suitable for investigating the combustion

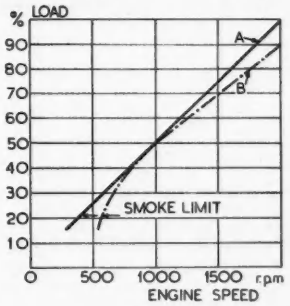

Fig. 2. **Smoke limit.**
Curve A. Variable advance angle, adjusted by hand.
Curve B. Constant advance angle.

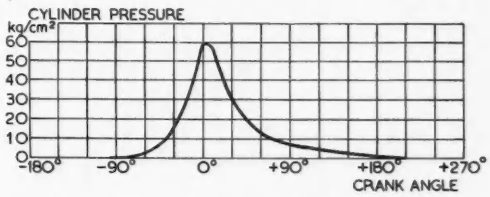

Fig. 3. **Pressure-time diagram taken at 1000 r.p.m. with multiple indicator ; 6·18 kg./sq. cm. m.e.p.**

process. A cathode ray oscillograph was therefore substituted and this proved much more suitable as will be seen from Fig. 4. Here the upper curve shows the pressure prevailing in the fuel line whilst the lower curve reproduces the pressure in the cylinder. Both pressures were recorded simultaneously, but it should be noted that the diagram scales are different. The first derivative of the pressure-time relationship was also recorded ; a typical oscillogram is shown in Fig. 5. The chart given in Fig. 6 demonstrates the influence of the engine speed upon the ignition delay, while Fig. 7 shows the influence of the advance angle upon the ignition delay at an engine speed of 1,500 r.p.m., the opening pressure of the injector being 90-140 kg. per sq. cm.

The demands of Swedish vehicle owners with regard to the silent running of engines are rather high, and

Fig. 4. **Oscillogram of cylinder pressure (lower curve) and fuel line pressure (upper curve) obtained with cathode-ray oscillograph.**

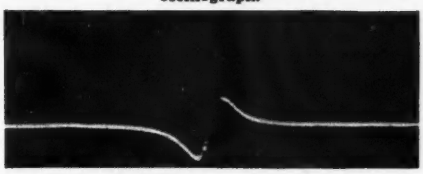

Fig. 5. **First derivative of pressure-time diagram.**

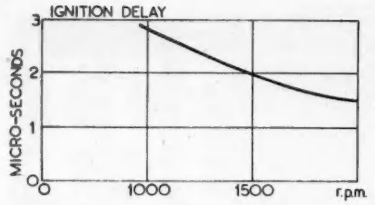

Fig. 6. **Influence of engine speed upon ignition delay.**

since it was desired to introduce the Volvo engine into the latest lorry type as quickly as possible, it was decided, in order to gain time, that the engine should be equipped with ante-chamber ; at the same time the development of the direct injection type was to be continued.

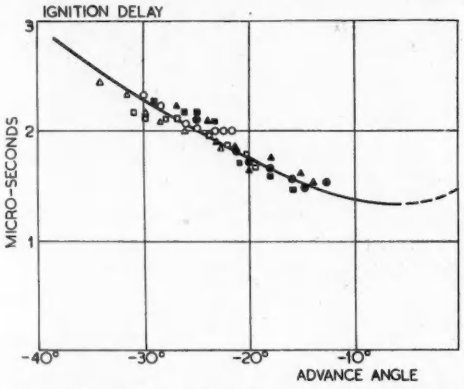

Fig. 7. **Influence of injection advance angle upon ignition delay at 1,500 r.p.m. and opening pressure of 90-140 kg./sq. cm.** Solid points refer to idling engine, others to full load.

In the case of an ante-chamber design the choice of the thermal loading of the ante-chamber and the cracking of the fuel are the main problems. It was found that the temperature characteristics of the ante-chamber are decisive in these respects and that both problems could be solved by giving the ante-chamber an appropriate configuration. In this way the maximum temperature in the ante-chamber could be lowered by 200 to 300 deg. C. as compared with conventional designs, and this without adversely affecting the fuel consumption.

The change-over from direct injection to ante-chamber injection furnished renewed proof of the fact that with the latter design ignition delay is smaller and remains almost constant with varying engine speed. It would appear that by appropriately adjusting the surface temperature of the combustion cavity and by providing a high degree of turbulence, ignition delay can be decreased to the minimum obtainable by any means.

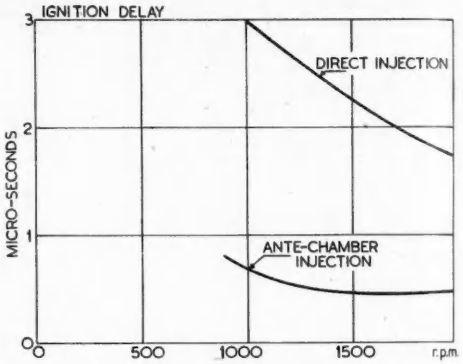

Fig. 8. **Ignition delay with direct and ante-chamber ignition respectively for varying engine speed.**

Fig. 8 shows that with the employment of an ante-chamber the ignition delay remains almost constant over the entire speed range of the engine. The employment of the advance angle control developed for the direct-injection engine could therefore be dispensed with. The salient data of the two engine types developed are as follows :—

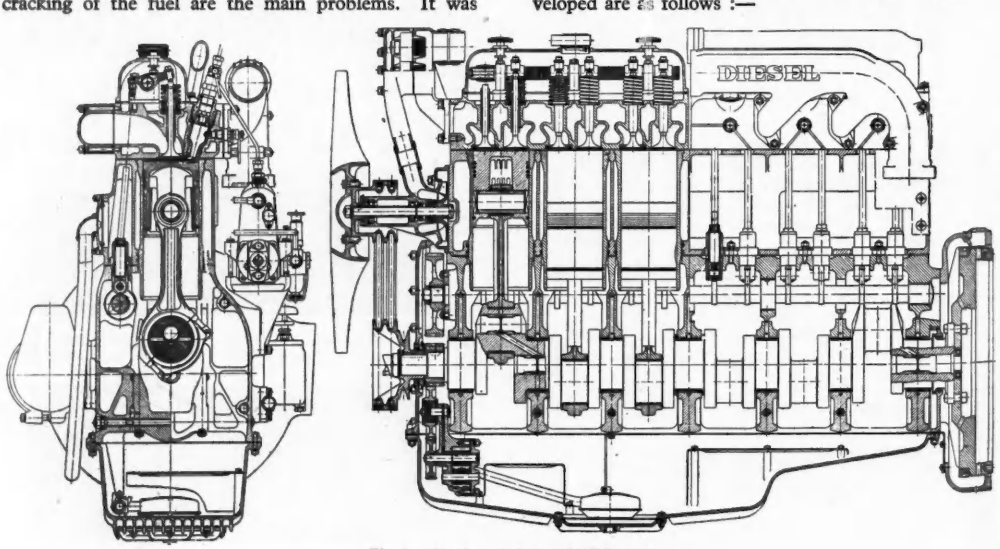

Fig. 9. **Sectional views of VDB engine.**

	VDA Design.	VBD Design.
Operating principle	4 cycle	4 cycle
Combustion space	Ante-chamber	Ante-chamber
No. of cylinders	6	6
Cylinder bore, mm	100	115
Stroke, mm	130	140
Working volume per cylinder, cu. cm.	1,021	1,454
Compression ratio	21	19
Firing order	1-5-3-6-2-4	1-5-3-6-2-4
Weight, complete without reduction gear box, kg.	about 580	about 640
Power developed at 2,000 r.p.m. e.h.p.	95	130
Maximum idling speed, r.p.m.	2,300	2,200
No. of crankshaft main bearings	7	7
Total journal area, sq. cm.	215	297
Journal diameter, mm.	82·55	100
Crank pin diameter, mm.	69·85	86
Port diameter :		
Admission valve, mm.	42	50
Exhaust valve, mm.	34	42

In the larger engine, that is, the VDB type shown in section in Fig. 9, the cylinder blocks of cast iron are connected with the light metal crank case by means of tie rods. The crankcase is strongly reinforced by ribs distributing the stresses. Both engine types are equipped with wet liners with double rubber packing between water space and crankcase. The pistons are of forged light metal and have three compression rings and two oil rings, the lower oil ring being placed below the gudgeon pin level.

The VDA type engine is equipped with a fuel pump in which the fuel delivery is controlled by variable stroke, while the fuel pump for the VDB type is equipped with spill-over port control operated by rotating the fuel pump pistons. The injectors open with a pressure of 100 kg. per sq. cm. and are equipped with sprayer nozzles of zero angle. Speed- and idling speed-control are effected by a vacuum control integral with the fuel pump, the vacuum control being operated from pressure variations in the induction pipe at a point immediately below the air filter. All bearings are of the lead bronze steel-backed type.

U. S. A.

An Electric Flow Meter

By J. H. LAUB*. (From *Electrical Engineering*, Vol. 66, No. 12, December, 1947, pp. 1216-1219, 6 illustrations.)

A NEW instrument for accurately measuring, recording, and controlling the rate of flow, as well as the total flow, of fluids applies an electrocaloric principle. A watt-meter is used to indicate and record the rate of flow and a watt-hour meter to register the total flow. The scale of the meter is linear and covers a very wide range.

THE ELECTROCALORIC METHOD.

If heat energy is introduced into or withdrawn from a medium flowing within a conduit and its temperature measured before and after the heat exchange the differential temperature Δt between the upstream and downstream thermometer readings will vary with the rate of flow. If Q denotes the heat flow in gram calories per second through the thin walls of a conduit of small diameter, M the rate of flow in grams per second, c the specific heat of the fluid in calories per degree centigrade per gram,

$$Q = c\,M\,\Delta t \qquad (1)$$

if heat losses by conduction and radiation can be neglected against heat convection by the fluid.

If Q is produced electrically in a heater coil wound in close thermal contact with the outside wall of the conduit and well-insulated otherwise, the wattage input W to the heater coil is proportional to Q,

$$W = k\,Q \qquad (2)$$

and eq. (1) becomes

$$W = kc\,M\,\Delta t \qquad (3)$$

and

$$M = \frac{1}{kc}\,\frac{1}{\Delta t}\,W \qquad (4)$$

From eq. (4) it follows that if the wattage input W were kept constant and the temperature differential Δt measured, the rate of flow M would be inversely proportional to Δt and would have to be read on a meter with a non-uniform, that is, hyperbolic, scale. If, however, the temperature difference Δt is kept constant by varying the wattage input W to the heater coil, the rate of flow M is proportional to W and can be read on the linear scale of the wattmeter measuring W. This can be accomplished if, instead of the two mercury thermometers, resistance thermometers are used and connected to a Wheatstone bridge circuit which is kept in balance for a given temperature difference Δt. If the balance is disturbed by a change in the rate of flow M, it is restored by adjusting the wattage input W to the heater coil, either manually or automatically. The resistance thermometers can be made, for instance, of nickel wire which has a high temperature coefficient of resistance and can be wound on the outside of the conduit in close thermal contact with its wall and well-insulated otherwise. A flow metering system thus is obtained, all of whose measuring elements are arranged outside of the fluid, which does not require conversion into an electric signal and which permits the rate of flow to be read on an instrument with a uniform infinite scale. It should be noted that this flow metering system causes much less pressure drop in the line than mechanical flow meters of the pressure drop type.

Furthermore, totalizing of the flow can be achieved simply by adding to the heater coil circuit a watt-hour meter which then will register the total quantity of the fluid which has passed through the meter. This follows from integrating both sides of eq. (4),

$$\int M d\tau = \frac{1}{kc}\,\frac{1}{\Delta t}\int W d\tau \qquad (5)$$

if τ denotes the time.

The left side of eq. (5) represents the totalized flow which is seen to be proportional to the wattage W integrated over any period of time and can be measured by a watt-hour meter.

Thus, we have arrived at a caloric electric system for measuring rate of flow as well as total flow, the basic elements of which are illustrated in Fig. 1. A tube section 1 of a metal with high heat conductivity is inserted into the fluid line and thermally insulated from it by insulating spacers 2. On it are wound a heater coil 3 and the downstream resistance thermometer 4, both in intimate thermal contact with the outside wall of section 1 and well-insulated otherwise. The upstream resistance thermometer 5 is wound on the outside wall of the fluid line and is separated from section 1 by one of the insulating spacers. Thermometers 4 and 5 form two arms of a Wheatstone bridge, the circuit of which is completed by two fixed and thermo-constant resistors 6 and 7, respectively, and by a Null indicator 8. In series

*Charles Engelhard, Inc., East Newark, N.J.

with the heater coil 3 are connected a current regulator 9 which may be operated automatically from the Null indicator 8, a wattmeter 10 calibrated to read rate of flow, for instance in pounds per hour, and a watt-hour meter 11 which registers the totalized flow, for instance, in pounds.

SHUNT ARRANGEMENT.

If large quantities of a fluid are to be measured, a substantial wattage would be required to maintain a satisfactory temperature differential Δt with the arrangement of Fig. 1. This would necessitate a heater coil of large dimensions and thus introduce an objectionable time lag. Instead, the arrangement illustrated in Fig. 4 is used for larger flows. A portion of the flow is shunted through a by-pass into which is inserted the section 1 carrying the heater coil 3 and the downstream thermometer 4, again heat-insulated by means of spacers 2. The upstream thermometer 5 now is wound on the main line and thermometers 4 and 5 again are connected into a Wheatstone bridge.

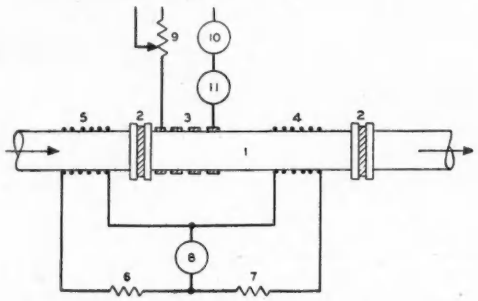

Fig. 1. **Basic elements of an electrocaloric flow meter.**

A small positive pressure head is maintained between inlet and outlet of the shunt by means of an orifice inserted in the main line a short distance ahead of the outlet.

TEMPERATURE COMPENSATION.

So far we have not considered the effect of varying fluid temperatures on the accuracy of flow measurements with the electrocaloric method. Referring again to eq. (3) we note that wattage W and flow rate M are proportional as long as the specific heat of the fluid remains constant. The latter is practically constant within a wide range of temperatures for most gases but varies somewhat for most liquids.

Furthermore, we have to consider the effect of temperature on the viscosity of the fluid. It increases for gases and decreases for liquids with increased temperature, and thus affects, to a certain extent, the character of the flow and the mechanism of the heat transfer between the coils and the fluid. Without going into the details of the rather involved theory of fluid flow and heat transfer in pipes, a reminder that the local velocity of the fluid within a conduit is by no means uniform must be sufficient.

It is obvious, therefore, that the heat transfer from the wall to the fluid is affected by the character of the flow in the neighbourhood of the wall, that is, by the temperature of the fluid. As a result of this, a flow meter as described so far shows a considerable temperature error. Fortunately, the latter practically can be eliminated by the simple and purely electrical compensation shown in Fig. 2. A small coil 12 of wire with a high temperature coefficient of resistance, for instance, nickel, is wound on the conduit and in intimate thermal contact with it. It is connected in series with the constant resistor 6 in one branch of the bridge and, as its resistance varies with the temperature of the fluid, the over-all effect is a slight shift of the bridge balance with temperature.

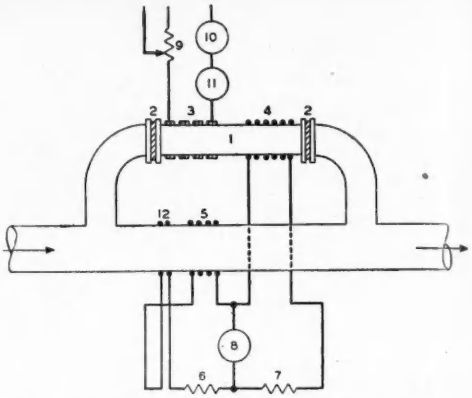

Fig. 2. **By-pass flow meter with temperature compensation.**

Variations of the ambient temperature will not affect the meter if the coils are heat-insulated well from the surrounding air and if the entire " transmitter " is enclosed in a metal cover which is in good heat-conducting contact with the pipe fittings and the fluid.

AUTOMATIC ELECTRONIC CONTROL.

Rebalancing of the bridge is accomplished automatically by a simple electronic circuit. It consists essentially of a voltage and power amplifier in series which step up the signal from the a.c. bridge sufficiently to operate a 2-phase reversible induction motor which drives the rheostat that regulates the current to the heater coil. The second phase of the motor is energized from the a.c. supply line, its current being displaced 90 degrees from the current in the first phase by means of a capacitor connected in series with it. As is well known, this arrangement has phase discriminating characteristics and the motor will reverse its direction of rotation when the signal from the bridge goes through zero and reverses its phase.

A similar arrangement is used for automatic control of the flow. In this instance the motor regulates a valve in the fluid line instead of driving the rheostat which then is set at a predetermined value corresponding to any desired rate of flow.

It should be noted also that fluctuations of the line voltage will not cause any error in indication. If, namely, the voltage varies the automatic control immediately will restore the wattage input to the heater coil which is demanded to maintain the fixed temperature differential Δt for a given rate of flow.

An example of the new electrocaloric flow meter is an instrument (illustrated in the original article) designed to measure the rate of flow and the total flow of aviation gasoline with a range from 0 to 2,000 pounds per hour. The transmitter consists of a by-pass arrangement with a 1-inch diameter main line and a 5/8-inch diameter shunt on which the heater coil of nichrome wire is wound. The maximum input to the latter is 50 watts corresponding to a flow rate of 2,000 pounds per hour. It is measured by a long scale indicating wattmeter calibrated in pounds per hour. The watt-hour meter registers the total flow and is calibrated in pounds and the two instruments are mounted in the hinged front panel of the receiver case. The electronic control unit consisting of amplifier, motor, and rheostat is mounted inside of the case on the rear panel and is easily accessible.

The Calculation of the Most Favourable Working Conditions for Chip Producing Machining Operations

By J. WITTHOFF. (From *Werkstatt und Betrieb*, Vol. 80, No. 4, April, 1947, pp. 77-84, 4 illustrations.)

FUNDAMENTAL RELATIONS.

A. THE DETERMINATION OF PRODUCTION COSTS.

I. The development of an equation of cost.

IT is usual to assess production costs as the sum of the wages paid and an amount which covers all other necessary charges. This, however, is not correct in principle and is quite inadequate for obtaining even an approximate comprehension of cost fluctuations due to changes in working conditions.

To be more precise, it is necessary to consider in detail the separate costs of which the production costs C_p, are built. These are the charges for wages C_w, tools C_t, energy C_e, "calculated" depreciation C_d, i.e. when part of depreciation used for cost calculation, maintenance C_m, and a remaining general cost C_g.

Thus $C_p = C_w + C_t + C_e + C_d + C_m + C_g$.

Some of these costs depend on, and others are independent of, changes in working conditions, but only those in the first category, denoted by C_v, are of interest whilst those independent of changes are not taken into account.

Production cost can only be determined approximately one of the reasons being that the "calculation" of depreciation costs which are nearly always based on the useful life of a machine, is very difficult to estimate with a reasonable chance of exactitude.

Costs in the category which do not necessitate further reference can be disposed of by the following :—

(1) If E is the consumption of energy of the machine tool to produce a certain amount of chips and e is the expenditure per unit of energy $C_e = E \times e$.

A change of working conditions affects that part of E, which is used during the time t_c, that is, during actual cutting. This part of E may be denoted by E_c. If N_c is the amount of work necessary for chip production, P is the main cutting force, p_s is the specific cutting pressure, and η is the efficiency of the machine during the cutting process, then

$$E_c = \frac{N_c t_c}{\eta} = \frac{P v t_c}{\eta}$$

where v is the cutting speed.

The work done by a lathe to cut a diameter d through a length l is $N_c = a \times f \times p_s \times v$ where a is the depth of the cut and f is the feed used.

However, $t_c = \pi d l / f v$ therefore $E_c = a p_s \pi d l / \eta = a \pi d l p_s / \eta$.

a, π, d and l are constant in this example, and p_s and η can also be considered constant above a certain loading of the lathe. Consequently the same applies to E_c, e and C_e.

(2) The useful life of a machine tool is determined by the amount of work it can do. It is independent of the period of time over which the work is distributed and is practically unaffected by maintenance. One is justified, therefore, to consider C_d and C_m as constants, particularly if the uncertainty in the determination of these two types of costs is taken into account. To consider C_d and C_m as being proportional to the production time is quite incorrect.

(3) The last term of the cost equation, C_g, contains the "calculated" interests. It would be possible to separate these and to determine them more accurately but the amount involved is comparatively small and its influence upon the final result is negligible.

Resulting from these considerations

$$C_v = C_w + C_t + C_g \quad .. \quad .. \quad (1)$$

Assuming a production of z pieces in a working time T_z including lost and supplementary times we obtain

$$\left.\begin{array}{l} C_w = W_p \times z \text{ for a piece work wage } W_p \\ \text{and} \quad C_w = W \times T_z \text{ for a fixed hourly rate } W \end{array}\right\} \quad (2)$$

To simplify the following cost comparison only a fixed hourly rate of wages is considered.

To determine time T_z it is necessary to know

t_{ch} the change-over time*.
t_s the supplementary time.
t_m the main time.
t_t the time necessary for tool changing.
T the life time of the tool.

t_{ch}, t_s, and t_m should each contain an allowance for lost time and refer to one unit of production.

$$T_z = t_{ch} + z\left(t_s + t_m + \frac{t_c}{T} t_t\right) \quad .. \quad (3)$$

Times t_m and t_c can be very accurately calculated if the dimensions of the work piece and the cutting conditions are known.

The work done by machine tools of the rotary type must be considered separately from that done by machines having reciprocating cutting motions.

(a) For rotary cutting action $t_m = \dfrac{\pi d l}{f v}$

which can in most cases be expressed with sufficient accuracy by $t_m = t_c$.

(b) Symbols used in connection with reciprocating cutting motions are dashed to distinguish them from those under (a). Let l_s denote the length of the total stroke and v_r the speed of the return stroke, then

$$t_m' = \frac{l l_s}{f}\left(\frac{1}{v} + \frac{1}{v_r}\right)$$

For broaching machines $l_s = f$ and $v_r = 0$,

$$\text{therefore} \quad t_m' = \frac{l}{v}$$

Assuming the ratio v_r/v is constant

$$t_m' = \frac{l l_s}{f v}\psi \quad \text{where } \psi = 1 + \frac{v}{v_r}$$

t_c' is usually much smaller than t_m'. With the usual approach and overrun

$$t_c' = \frac{l l_s}{f v}$$

Thus equations for t_m, t_m', t_c, and t_c' apply to the conditions for one cut and for several cuts the results should be multiplied accordingly.

Under certain circumstances t_m, t_c and t_t may correspond to several operations and tools.

(2) If C_{lt} is the tool costs during the life time T of the tool, n_T is the number of tool life times per tool, V_a is the initial value of the tool before being ground for use, V_z is the value of the tool when it can no longer be used for the production under investigation, and C_s is the cost of sharpening the tool once, then the equation relating these quantities is

*An exact definition of the various "times" is given in the book, "Time Study and Rate Fixing," published by Engineers' Digest Ltd. and Sir Isaac Pitman & Sons, Ltd., London.

$$C_{lt} = \frac{1}{n_T}(V_a - V_s) + C_s.$$

C_{lt} is constant for certain tool types assuming that the wear of the individual tools is equal.

$$\text{Therefore } C_t = \Sigma\left(\frac{t_c \times z}{T} \times C_{lt}\right) \quad .. \quad (4)$$

(3) The remainder of the general production cost per unit of calendar time and per machine tool, is denoted by c_g. The shift-time factor i.e. the ratio of the shift-time to the calendar time is β_s and the production time factor, i.e. the ratio of the production time to the shift-time is β_p.

$$C_g = \frac{c_g}{\beta_s \beta_p} T_z \quad .. \quad .. \quad (5)$$

From eqs. (1), (4), and (5)

$$C_v = \left(W + \frac{c_g}{\beta_s \beta_p}\right) T_z + \Sigma\left(\frac{t_c z}{T} C_{lt}\right)$$

For production with a single tool $z = 1$. The bracketed quantity in this equation is a constant, denoted by C_1, so that

$$C_v = C_1 T_z + \frac{t_c}{T} C_{lt} \quad .. \quad .. \quad (6)$$

C_1 is constant for a certain production even if the working conditions vary.

II. Transformation of the Cost Equation.

By combining eqs. (6) and (3)

$$C_v = C_1\left(\frac{t_{ch}}{z} + t_s\right) + C_1 t_m + \frac{t_c}{T}(C_1 t_t + C_{lt})$$

in which

(1) $C_1\left(\frac{t_{ch}}{z} + t_s\right)$ is practically invariable

(2) t_m is a function of $\frac{1}{fv}$

$$C_1 \frac{\pi d l}{f v} = C_2 \frac{1}{f v} \quad \text{where} \quad C_2 = \pi d l C_1$$

Correspondingly for machine tools, with reciprocating movement

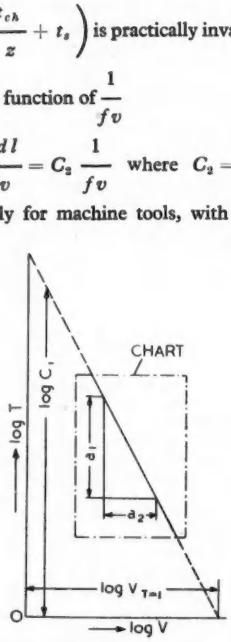

Fig. 1. Determination of c_1.

$$C_2' = l l_c \psi C_1$$

(3) The quotient t_c/T is proportional to $1/fvT$. The relation between T and v for given cutting conditions, especially for a given value of f, can be seen from the life-time curve which is a straight line when plotted on a log-log chart. This means that $T = c_1 v^{c_2}$, c_1 and c_2 being constants. c_2 represents the slope of the life-time curve and is always negative. Therefore

$$\frac{t_c}{T}(C_1 t_t + C_{lt}) = \frac{\pi d l}{v c_1 v^{c_2}}(C_1 t_t + C_{lt}) = \frac{C_3}{c_1 f v^{c_2+1}}$$

Similarly

$$\frac{t_c'}{T}(C_1 t_t + C_{lt}) = \frac{C_3'}{c_1 f v^{c_2+1}}$$

Therefore

$$C_v = C_1\left(\frac{t_{ch}}{z} + t_s\right) + \frac{C_2}{fv} + \frac{C_3}{c_1 f v^{c_2+1}} \quad .. \quad (7)$$

$$\text{and } Cv' = C_1\left(\frac{t_{ch}}{z} + t_s\right) + \frac{C_2'}{fv} + \frac{C_3'}{c_1 f v^{c_2+1}} \quad .. \quad (7')$$

B. Determination of the Working Time.

The working time is already given by eq. (3). With

$$C_4 = \pi d l$$
$$C_4' = l l_c \psi$$
$$C_5 = \pi d l t_t$$
$$C_5' = l l_c t_t$$

results are obtained for $z = 1$ in the same way as in section A.

$$T_z = \frac{t_{ch}}{z} + t_s + \frac{C_4}{fv} + \frac{C_5}{c_1 f v^{c_2+1}} \quad .. \quad .. \quad (8)$$

$$T_z' = \frac{t_{ch}}{z} + t_s + \frac{C_4'}{fv} + \frac{C_5'}{c_1 f v^{c_2+1}} \quad .. \quad (8')$$

THE DETERMINATION OF THE MOST FAVOURABLE WORKING CONDITIONS.

A. Working Conditions Giving the Lowest Production Costs.

I. Calculation of the cutting speeds which result in the lowest costs.

The following is relevant to machines having a revolving main movement ; machines with a reciprocating main movement can be treated similarly.

The structure of eq. (7) shows that the C_v curve for a definite value of f plotted against v must have a minimum. The cutting speeds relating to the smallest values of C_v and C_v' i.e. C_{v_0} and $C_{v_0'}$, are denoted by v_0 and v_0'. Differentiating eq. (7) with respect to v, and equating to zero

$$\frac{d C_v}{d v} = -\frac{C_2}{f v^2} - (c_2 + 1)\frac{C_3}{c_1 f v^{c_2+2}} = 0$$

and substituting for C_2 and C_3, the following values are obtained for v_0 and v_0' :—

$$v_0 = \sqrt[-C_2]{\frac{c_1 C_1}{(C_1 t_t + C_{lt})(-c_2 - 1)}} \quad .. \quad (9)$$

$$v_0' = \sqrt[-C_2]{\frac{c_1 C_1 \psi}{(C_1 t_t + C_{lt})(-c_2 - 1)}} \quad .. \quad (9')$$

By introducing these values into the equation $T = c_1 v^{c_2}$ we obtain

$$T_0 = \left(t_t + \frac{C_{tt}}{C_1} \right) (-c_2 - 1) \quad .. \quad (10)$$

and $$T_0' = \frac{1}{\psi} \left(t_t + \frac{C_{tt}}{C_1} \right) (-c_2 - 1) \quad .. \quad (10')$$

T_0 and T_0' can easily be calculated and the determination of c_1 is no longer necessary. First T_0 and T_0' should be ascertained and then, for these values, v_0 and v_0' should be read from the life-time curves.

Eqs. (9) and (10) make it possible to calculate the most economical cutting speeds v_0 and v_0' for a certain kind of production after the correct feed has been chosen. v_0 and v_0' are independent of the dimensions of the work-piece.

When machining given work-pieces with certain depths of cuts and with tools of a particular type and of a certain material, the cutting angles remain substantially unchanged. In such cases the life-time curves are usually parallel to each other for different feeds, i.e. c_2 remains unchanged. The equations of the life-time curves only show differences in so far as c_1 decreases with increasing feed. Therefore v_0 and v_0' decrease with increasing feed all other working conditions remaining unchanged. These considerations also hold good in principle for machines working with several tools.

II. Selection of the Most Economical Feed.

A simple expression is obtained for the value of C_{v_0} corresponding to v_0 if v_0 is introduced into eq. (7).

$$C_{v_0} = C_1 \left[\frac{t_{ch}}{z} + t_s + \frac{\pi d l}{f v_0} \left(1 + \frac{1}{-c_2 - 1} \right) \right] \quad (11)$$

Similarly

$$C_{v_0}' = C_1 \left[\frac{t_{ch}}{z} + t_s + \frac{l l_s \psi}{f v_0} \left(1 + \frac{1}{-c_2 - 1} \right) \right] \quad (11')$$

C_{v_0} is smaller as the product fv_0 is larger. Since C_1, t_t, C_{tt}, and c_2 do not change, v_0 is proportional to $\sqrt[-c_2]{c_1}$ and $-c_2$ is never less than 4, for the usual life-time curves. Thus the decrease of v_0 is considerably less than the amount of increase of f. Consequently the value of C_{v_0} is smaller as f is larger. In other words, feeds as large as possible should be used to obtain smaller production costs.

III. Mathematical Procedure.

Feed increase is limited by the quality of the surface required and by the capacity of the tool and the machine. It is especially important not to use feeds so large as to damage the cutting edges, as this would result in a considerable decrease of c_1, an increase of C_{tt} and C_3 and consequently in a considerable increase of C_{v_0}.

The power consumption of the machine tool is proportional to v_0, as well as to f, and, especially with the latter, changes the specific cutting pressure p_s. Thus high feeds allow of full utilization of the machine tool capacity and of an increase in the mechanical efficiency η_m. Whether the driving power is sufficient, should be checked by the equation

$$N = \frac{a f p_s v}{\eta_m}$$

where N denotes the power of the motor necessary for chipping. If it is found that N is too high in comparison with the rated motor power N_m the feed f must be lowered. This also means an increase of p_s in most cases.

If the feed f is chosen, the most economical values of the cutting speed v_0 at the minimum production cost C_{v_0} depending on the working conditions, and the life-time of the tool T_0 at the speed v_0, should be determined ; for this purpose c_1, c_2, C_1, t_t, C_{tt} and ψ must be known.

(1) c_1 and c_2 can be determined from a life-time curve. Such curves can either be found in the existing literature or developed from simple experiments. Their course depends on the material to be machined, especially on the condition of the layers to be removed, on the tool material, the cutting angles, the depth of the cut, the feed and the type of coolant.

c_2 is the tangent of the angle of inclination of the life-time curve. As already mentioned it is always negative. c_1 corresponds to T when $\log v = 0$ (see Fig. 1.) Because it is usually not possible to draw the co-ordinates on the usual size of paper, $\log c_1$ is determined from the relation $\log c_1 / \log v_{T=1} = a_1/a_2 = c_2$ where $v_{T=1}$ is the speed for a life-time $T = 1$ minute, and a_1 and a_2 are explained by Fig. 1. Therefore, $\log c_1 = \log v_{T=1} \times c_2$. $\log v_{T=1}$ can be ascertained from the life-time curve by taking into consideration its inclination and the scale on the abscissa. The actual course of the life-time curve near the co-ordinates does not affect the correctness of the results obtained.

(2) $C_1 = W + \frac{c_g}{\beta_s \beta_p}$. c_g denotes the general production cost per unit of calendar time and per machine. It is determined in the usual way by employing a suitable key to allocate the indirect or general costs to the production under investigation. β_p and β_s are the time factors of the production time as a whole and of the shift time respectively ; β_p must be estimated.

(3) An average value should be used for t_t ; this can easily be determined.

(4) The same applies to the value of C_{tt}.

(5) ψ is constant only if the drive of the rectilinear main movement is caused by a crank gear. However, it has also been determined for some other types of drive for planing machines. Figures obtained in the most unfavourable case of a ram planer with hydraulic drive, fluctuated very considerably between 1·2 and 2, and the determination of ψ in such a case is therefore based more or less on a method of trial and error. For a certain range of v, within which ψ does not fluctuate too much and which is likely to contain v_0', v_0' is calculated from an assumed value of ψ. Should v_0' be found to be outside the range originally suggested, the calculation must be repeated using other values, until the determined value of v_0' lies within the assumed limits.

IV Mathematical Means for the Evaluation of v_0 and v_0'

Logarithamic calculations cannot be avoided for this.

(1) Slide rule accuracy is sufficient. First the term under the root in eqs. (9) and (9') has to be determined in the usual way. Let this be denoted by R then,

$$v_0 = \frac{1}{-c_2} \log R.$$

(2) The use of a series of nomograms is recommended, each nomogram introducing one additional variable, as shown in Fig. 2.

V. Influence of Inaccuracies in Factors Determining v_0 and v_0'.

As the value of $-c_2$ usually fluctuates between 4 and 18, v_0 and v_0' are comparatively insensitive to alterations of the radicand in eqs. (9) and (9'). Especially with machine tools having a rectilinear main movement inaccuracy of ψ does not impair the usefulness of the calculation, especially because it is not often possible to adjust such machines for the exact calculated cutting speed.

On the other hand inaccurate values of c_2 are of considerable importance, and it is therefore necessary to determine c_2 as exactly as possible. This is greatly facilitated if the life-time curves for different feeds are parallel.

B. Determination of the Working Conditions for the Shortest Working Time.

If it is required in special cases to obtain the shortest possible working time T_z the procedure is the same as explained in section A, i.e. eq. (3) for T_z must be differentiated and the differential quotient equated to zero. The resultant cutting speeds v_{Tz_0} and v_{Tz_0}' can be calculated as follows :—

$$v_{Tz_0} = \sqrt[-c_2]{\frac{c_1}{(-c_2-1)\,t_t}} \quad .. \quad .. \quad (12)$$

and

$$v_{Tz_0}' = \sqrt[-c_2]{\frac{c_1\,\psi}{(-c_2-1)\,t_t}} \quad .. \quad .. \quad (12')$$

It is useful to determine the life-time T_{Tz_0} and T_{Tz_0}' for the shortest working time and to take v_{Tz_0} and v_{Tz_0}' from the life-time curves.

$$T_{Tz_0} = (-c_2-1)\,t_t \quad .. \quad .. \quad (13)$$

$$T_{Tz_0}' = (-c_2-1)\,t_t/\psi \quad .. \quad (13')$$

With regard to the calculation for the development of a nomogram and to the accuracy of results, the same considerations can be applied as in Section A. The factors necessary for the determination of v_{Tz_0} and v_{Tz_0}' (eqs. (12) and (12')), are bracketed in Fig. 2. The readings start in the second alignment chart from the value $1/t_t$.

C. Discussion of the Results.

By transforming the radicand in eq. (9) into

$$\frac{c_1}{\left(t_t + \frac{C_{tt}}{C_1}\right)(-c_2-1)}$$

it is clear that v_0 is larger for given life-time conditions as t_t and C_{tt} are smaller. Thus, a production with a quick change of tools, or with cheap and easily sharpened tools requires a comparatively high cutting speed from the economic point of view. Short life-times have no great influence on the cost. It is the reverse in the case of operations, requiring a long time for tool changing and expensive tools. In such cases high life-times and small cutting speeds are economical. Often it is found that contrary to the opinion of the workshop, the originally intended cutting speed should be considerably decreased for economic reasons. If the sum of wages and overheads is relatively high, especially when very expensive machine tools are used, a high v_0 is recommended, even if that means increased expenditure for tools. These comparisons refer to the use of the same tool material. If, however, different cutting materials are compared with each other, preference should be given to a material which allows for higher cutting speeds with the same life-time. That is the reason for the economic superiority of hard metal compared with high speed steel.

The figures for v_{Tz_0} increase as t_t decreases. For, a decrease of the working time by an increase in the cutting speed is more pronounced in its effect if individual tool change times are reduced because the number of changes necessary increases greatly with increased cutting speeds and consequently reduced tool lives.

D. Examples.

1. *Rough Turning of Tubular bodies.*

A large number of tubular steel bodies of 90 kg /mm² strength are to be rough turned on a special forge lathe. v_0 and C_{v_0} are to be calculated for different feeds. The necessary data are given in Table I, column 2.

The feed selected can be as large as technically possible, but if it is more than 1·1 mm frequent breakage results. Therefore this value is used as the upper limit. Further calculations are for feeds of 0·9 and 0·7 mm, and Fig. 3 shows life-time curves A_1, A_2 and A_3 experimentally established for these feeds. Using indices

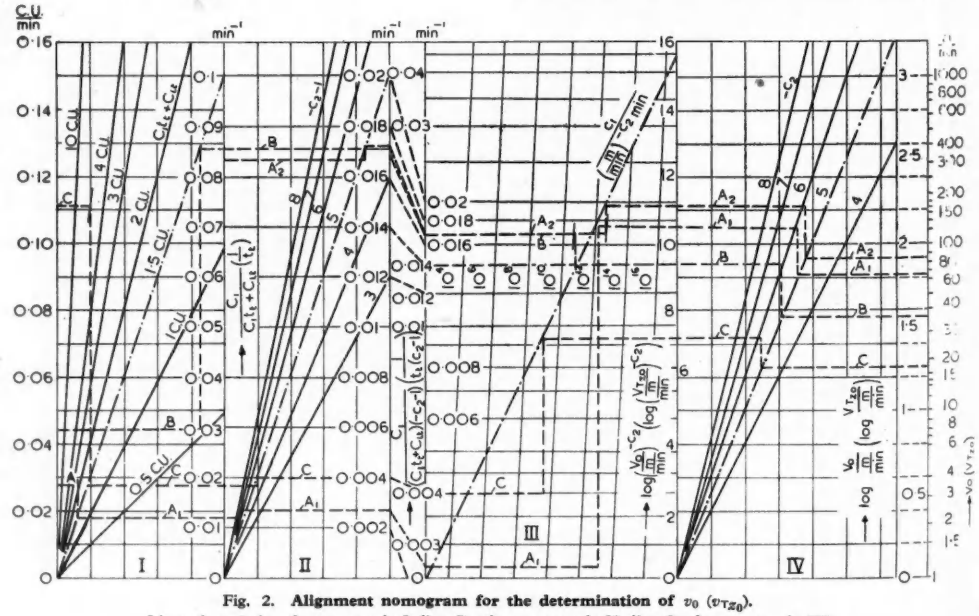

Fig. 2. Alignment nomogram for the determination of v_0 (v_{Tz_0}).
Lines A_1 and A_2 refer to example I, line B refers to example II, line C refers to example III.

1, 2 and 3 for these three feeds we can write

$$c_{z_1} = c_{z_2} = c_{z_3} = c_z = -5{\cdot}8$$

$$c_{1_1} = 9{\cdot}6 \times 10^{12}\,(\text{m/min})^{5{\cdot}8} \times \text{min}$$

$$c_{1_2} = 1{\cdot}35 \times 10^{13}\,(\text{m/min})^{5{\cdot}8} \times \text{min}$$

$$c_{1_3} = 2{\cdot}16 \times 10^{13}\,(\text{m/min})^{5{\cdot}8} \times \text{min}$$

Also $C_1 = \left(0{\cdot}78 + 4050\,\dfrac{1}{0{\cdot}62 \times 0{\cdot}85 \times 8760 \times 60}\right) =$

$= 0{\cdot}0277$ C.U.*/min

$$C_{1t} = \frac{1}{8} \times 12{\cdot}90 + 0{\cdot}24 = 1{\cdot}85 \text{ C.U.}$$

$$C_1\,t_t = 0{\cdot}0277 \times 12 = 0{\cdot}33 \text{ C.U.}$$

(1) For $f = 1{\cdot}1$

$$v_{0_1} = \sqrt[5{\cdot}8]{\frac{9{\cdot}6 \times 10^{12} \times 0{\cdot}0277}{(0{\cdot}33 + 1{\cdot}85)\,(5{\cdot}8 - 1)}} = 62 \text{ m/min}$$

$$C_{v0_1} = 0{\cdot}0277 \left[2{\cdot}2 + \right.$$

$$\left. + \frac{\pi \times 0{\cdot}116 \times 0{\cdot}38}{0{\cdot}0011 \times 62} \left(1 + \frac{1}{5{\cdot}8 - 1} \right) \right] = 0{\cdot}129 \text{ C.U.}$$

$$v_{Tz_0} = \sqrt[5{\cdot}8]{\frac{9{\cdot}6 \times 10^{12}}{12\,(5{\cdot}8 - 1)}} = 85 \text{ m/min}$$

(2) For $f = 0{\cdot}9$ mm, $v_{0_2} = 67$ m/min and $C_{v0_2} = 0{\cdot}139$ C.U.

(3) In the third case, i.e. for $f = 0{\cdot}7$ min, we get $v_{0_3} = 73$ m/min and $C_{v0_3} = 0{\cdot}152$ C.U.

The driving motor of the machine tool can produce the power necessary for a feed of 1·1 mm. For a specific pressure $p_s = 170$ kg/mm² and a mechanical efficiency of 50 per cent, the power necessary is

$$N = \frac{170 \times 5 \times 1{\cdot}1 \times 62}{0{\cdot}5 \times 60 \times 75 \times 1{\cdot}36} = 19 \text{ kW}$$

*All costs are given in Mark in the original German text. As it is impossible, at the present, to assess the value of German money we have put one Mark equal to one cost unit (C.U.)—Ed. E.D.

2. *Smooth Planing Cast Steel Work-Pieces.*

Cast steel of more than 70 kg/mm² strength should be finish-machined on a hydraulically-driven planer, the cutting speed of which can be varied between 4 and 40 m/min, and the return speed between 20 and 40 m/min. The most favourable working conditions should be established. All necessary data can be taken from column 3 of Table I. The quality of surface finish required sets the upper limit of the feed at 0·2 mm, for which feed the most economical cutting speed v_0 can be determined from the life-time curve B in Fig. 3. $c_z = -6$.

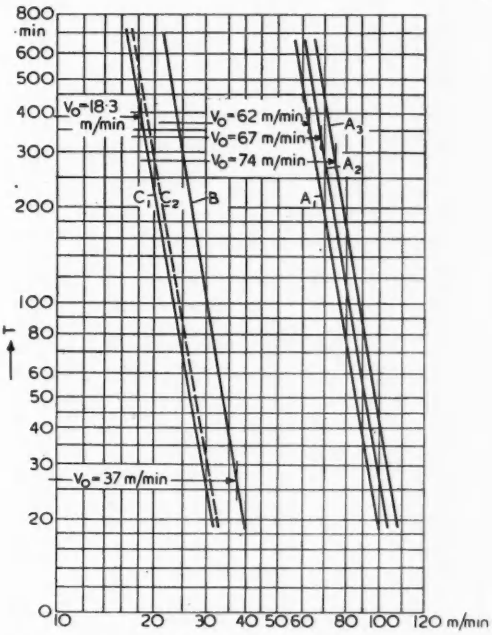

Fig. 3. **Life-time curves for examples I, II, and III referred to by A_1, A_2, A_3, B, and C_1, C_2 respectively.**

TABLE I. DATA FOR EXAMPLES I, II AND III.

1	2	3	4	
Description	Example 1	Example II	Example III	
WORK-PIECE				
Description	tubular bodies	casting	Locomotive tyres	
Material	basic Bessemer steel	steel	steel	
Strength	90 kg/mm²	above 70 kg/mm²	100 to 110 kg/mm²	
WORKING CONDITIONS				
β_s	0·62	0·57	0·48	
β_p	0·85	0·75	0·80	
c_g	4050 C.U./year	5800 C.U./year	18500 C.U./year	
MACHINE TOOL				
Description	special roughing lathe	hydraulic planer	wheel lathe	
Motor rating	22 kW	15 kW	29·5 kW	
			tread	*flange*
Number of tools	1	1	2	2
$V_{gt} - V_z$	12·90 C.U.	4·30 C.U.	13·30 C.U.	37·90 C.U.
C_g Cost of one sharpening	0·24 C.U.	0·10 C.U.	0·27 C.U.	0·40 C.U.
Number of life-times per tool	8	18	12	13
FIXED HOURLY RATE	0·78 C.U./hour	1·10 C.U./hour	1·20/C.U./hour	
PROCESS				
d and l_s respectively	116 mm	400 mm	1700 mm	
l	380 mm	600 mm	115 mm	
a	5 mm on the average	2 mm	5·5 mm on the average	
f	1·1, 0·9, 0·7 mm	0·2 mm	1 mm	
ψ	—	1·9 (assumed)	—	
t_t	12 min	4 min	5·5 min |	8·8 min
t_s	2·2 min	—	—	

$$\text{With } C_1 = \left(1{\cdot}10 + 5800\,\frac{1}{0{\cdot}57 \times 0{\cdot}75 \times 8760}\right) = 0{\cdot}044 \text{ C.U./min}$$

$$C_{lt} = \left(\frac{1}{18} \times 4{\cdot}30 + 0{\cdot}10\right) = 0{\cdot}34 \text{ C.U.}$$

and with an estimated value of $\psi = 1{\cdot}9$, it can be calculated, using eq. (10′) that

$$T_0' = \frac{1}{1{\cdot}9}\left[(4 + \frac{0{\cdot}34}{0{\cdot}044})(6-1)\right] = 30 \text{ min}$$

From the life-time curve B in Fig. 3 :—$v_0' = 37$ m/min. With this value we get

$$\psi = 1 + \frac{37}{40} = 1{\cdot}92.$$

The difference from the previously estimated value of 1·9 is negligible. The life-time T_0' is comparatively short. This can be appreciated with regard to the small tool costs and the short time necessary for tool changing.

III. Finish Turning Locomotive-Tyres.

The profiles of worn locomotive tyres are finish-turned on a wheel lathe which incorporates two copying devices. Each carriage has two tools working simultaneously, one machining the tread and the other the flange. A roughing tool is used for the tread, and a forming tool with a semicircular cutting edge for the flange. Thus 4 tools do the cutting required. 23·5 m/min was used as the cutting speed and 1 mm as the feed.

The separate steps of the calculation are not given here, but data are given in column 4 of Table 1. It may be mentioned, however, that the method of calculation explained above, can be applied in spite of the difference of the tools and their life-time. The necessary alterations make no difficulties and result simply from the given working conditions. The most economical cutting speed is $v_0 = 18{\cdot}3$ m/min, and, using the experimentally determined life-time curves C_1 and C_2 (see Fig. 3), the life-time is found at about 500 min. From the economical point of view a decrease of the applied cutting speed of 23·5 m/min could be recommended, because the share of the tool costs C_t in the total production cost C is comparatively high, and consequently high life-times are of special importance. On the other hand, the shortest working time of the machine can be obtained at a cutting speed of $v_{T_{z_0}} = 23$ m/min. The lower output of the machine with a cutting speed v_0 was balanced by increased loading of the lathe, which was possible without much trouble.

LOOKING AHEAD.

The method of calculation described does not require verification by experiments, because it is based on mathematical deductions. However, if it is used one must be sure, that the production is proceeding according to anticipated rules, especially in so far as actual chipping is concerned. This particularly refers to the problem of the life-time of the tools.

The article gives a fundamental insight into the costing conditions of chip removing processes, and shows how it is possible, in practice, to fix working conditions to obtain the smallest production cost, or the smallest production times. There is no doubt that these problems will be of special importance in the future. Suitable charts and data for facilitating calculations in practical cases, are being prepared.

The principles outlined in this article also apply to manufacturing processes without chip removal. Details in this connexion are reserved for future publications.

RUSSIA

Electrical Drives Without Reduction Gearing

By M. Yu. SHUHATOVICH. (From *Vestnik Inzhenerov i Tehnikov*, No. 7, 1946, pp. 212–216, 4 illustrations.)

DIRECT electrical drives are becoming more and more popular and there is an increasing tendency to merge the electrical and the mechanical portions of machinery together so that a single rotating part will do the required mechanical duty whilst acting as the motor armature at the same time.

This tendency should find its logical conclusion in a greater use of the arc stator, which was first proposed by P. Trombetta of the British Thomson Houston Company in 1924 and subsequently neglected, until it was recently developed into a successful commercial proposition by P. Fridkin* in Russia, who has proposed a modification known as the " axial arc stator."

The normal type of Stator, which forms a complete circle, can only give speeds determined by the formula (neglecting slip) :—

Speed $(n) = \dfrac{60f}{p}$ where f is the supply frequency and p is the number of pairs of poles.

Thus although it acts as a " reduction gear " between the electrical supply and the mechanical device it drives, it only gives reduction ratios which can be expressed by whole numbers.

The Trombetta-Fridkin stator, in which the stator occupies only an arc of a circle, gives a reduction ratio :—

$$Q = \frac{B}{P} \text{ where } B = \text{arc enclosure coefficient} = \frac{\text{angle of stator arc } (\phi) \text{ in radians}}{2\pi}$$

There is thus a freedom to choose reduction ratios which need not be whole numbers and, in the case of large reduction ratios, a considerable simplification of construction and saving in costs can be obtained.

The same basic principle has been applied by A. Imas (1940) in his " Helical " stator, shown in Fig. 1, which covers an angle greater than 2π and therefore, if wound with a single pair of poles, will give a speed in

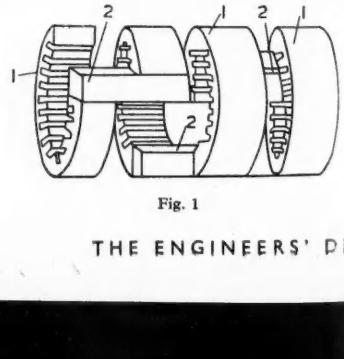

Fig. 1

* See P. A. FRIDKIN : " Theory of the Arched Stator Drive," THE ENGINEERS' DIGEST, Vol. 6, No. 11, pp. 281–286, Ed. E,D,

excess of the supply frequency (i.e., greater than 3000 r.p.m. with a 50 cycle supply). In this case also the reduction ratio is infinitely variable according to the total angle of the "helix." In fact, there is no theoretical difference between this and the arc stator, so that there is reason to wonder why Trombetta and Fridkin did not realize the "stepping-up" possibilities of their device, and Imas was apparently unaware that his invention was only a logical extension of the arc-stator principle.

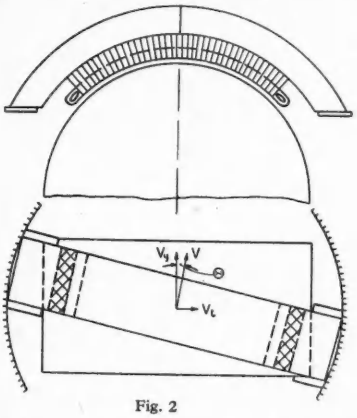

Fig. 2

Finally if we put the stator "on the skew" relatively to the axis of rotation of the rotor (see Fig. 2) a further variation of the reduction ratio is obtained which Fridkin has proposed to utilize in his "axial-arc stator." If the angle Θ between the plane of the stator windings and the rotor axis is small the "reduction gear" obtained is somewhat similar to that of a worm gear. (Close inspection of Fig. 2 will show this; and it will be noted that, although at a first glance it appears to depart very little from Fig. 1, the windings of the stator run *lengthwise* along the arc so that the angle Θ is very small instead of 90 deg. as in the normal Trombetta stator).

The general formula for all the stators so far discussed is :—

$$\text{Reduction ratio } Q = \frac{B}{P} \sin \Theta$$

$$\text{and } n = 60 f \times Q.$$

From these formulæ :—

1. If $B = 1$ and $\sin \Theta = 1$
   — a normal motor with a full-circle stator.
   $$n = 60 \frac{f}{p}$$
2. If B is less than 1 and $\sin \Theta = 1$
   — the Trombetta arc stator
   $$n = 60 f \frac{B}{P}$$
3. If B and $\sin \Theta$ are both less than 1
   — the Fridkin "axial arc" or "worm-gear reduction" stator
   $$n = 60 f \frac{B}{P} \sin \Theta$$
4. If B is greater than 1 and $0 < \sin \Theta < 1$
   — the Imas "helical" stator

In addition it is possible to imagine two further types: "axial full circle" and "axial helical."

So far we have regarded all stators as differing only with respect to B and Θ. But from this practical point of view the various "special" designs differ from the normal stator also because they are asymmetrical and their magnetic systems are, as it were, incomplete or "open ended."

The geometrical asymmetry leads to the magnetic field being elliptical, which is not of great importance during steady running, but increases the rated current and reduces starting torque. Another effect is that instead of pure torque we now get also a magnetic force F acting on the rotor, where

$$F = 0{\cdot}5 \left[\frac{B_e}{5000}\right]^2 KDS \sin B\pi$$

The "open-ended" form of the stator results in end effects which have a braking action and increase the current consumption of the stator. It appears that Fridkin has largely succeeded in overcoming this trouble, because his rated efficiencies and slip for arc stators are much the same as for motors with circular stators.

The asymmetry of field and shape, therefore, leads to a number of difficulties and uncertainties in design calculations, which probably account, more than any other factor, for their slow development. Another difficulty regarding the ordinary arc stator of the Trombetta type is that the peripheral velocity of the rotor must not be less than 11–12ft./sec., which makes it unsuitable for use in much mining and similar slow-moving equipment where its application would otherwise be attractive.

As against these difficulties of design, one advantage which can be mentioned is that the heat developed in the rotor is given up mainly to the atmosphere and not to the stator, so that it is unnecessary to distribute the rotor energy losses, and high-resistance rotor windings can be adopted.

Fridkin and Berenov have designed a winding gear with an arc stator and a 23 ft. diameter flywheel which acts as the rotor with a peripheral speed of 41 ft./sec. This machine can develop a power of 800 kW, has an efficiency of 88 per cent, and possesses very good starting characteristics, although the power factor (65 per cent) is lower than it would have been with a normal full-circle stator as is usually the case with modern arc-stator designs. The speed of the winding gear can be regulated by varying the number of turns in the stator winding by changing the neutral point of its star connection. The rotor winding is permanently short circuited, as is nearly always the case with arc-stator machines. An alternative way of regulating the speed of these machines is by introducing an auto-transformer in the stator circuit.

The main advantages of arc-stator driven machinery are :—

1. Mechanical simplification due to the abolition of reduction gearing.
2. Considerable reduction in weight (25–30 per cent).
3. Considerable reduction in cost.
4. Saving in production and erection times.
5. Reduction in running costs due to simplicity, smaller current consumption, simpler lubrication and fewer spare parts.
6. Smooth and silent running.

These advantages are sufficient to justify much more research, than is carried out at present, to study the magnetic properties of the arc-stator field and the behaviour of arc-stator machinery under conditions of sudden load variations and greatly varied speed.

The construction of experimental installations on something like a commercial scale is also very desirable at this stage.

For machinery with peripheral speeds below 12 feet per second, the application of the arc-stator principle will have to depend on the success of Fridkin's axial-arc or "worm-gear" designs which require much more scientific and practical study.

U.S.A.

The Use of the Expansion of Gases in a Centrifugal Field as Cooling Process*

By R. HILSCH, Institute of Physics, Erlangen, Germany. (From *The Review of Scientific Instruments*, Vol. 18, No. 2, February, 1947, pp. 108-113, 5 illustrations.)

1. INTRODUCTION.

THE design of a vortex tube of good efficiency in which the expansion of a gas in a centrifugal field produces cold is described, and the maximum efficiency obtainable is determined. In Ranque's original arrangement, air entered through a tangential nozzle into a tube of 12 mm diameter. A turbulent flow of gas, in a screw-like motion, escapes through both ends. This rotating air stream produces a region of increased pressure near the wall inside the cylinder, and a region of decreased pressure near the axis. If one end of the cylinder is closed by a diaphragm which permits the escape of air only from the central region, while the other end is throttled, the air escaping through the central diaphragm has a reduced temperature, whilst the air escaping through the other end shows a temperature increase. The temperature difference observed between the two streams, using compressed air of 6-atmos. gauge pressure at 20 deg. C., was 70 deg. C., while the lowest temperature of the cold stream was — 12 deg. C.

2. CONSTRUCTION AND FUNCTION OF A "VORTEX TUBE."

The results of numerous preliminary experiments showed that for a favourable cooling effect the diaphragm should be installed as near as possible to the nozzle. The circular air flow near the nozzle and the diaphragm should be as nearly as possible of rotational symmetry. This is achieved by a peculiar method of introducing the compressed air, which is shown in Fig. 1b and 1c. Two pieces of tubing of internal diameter R are attached to the cylinder by means of flanges and overlapping nuts ; one of the flanges acting as diaphragm B located near the nozzle.

For an explanation of the mechanism of the vortex tube we refer to Fig. 1a. If both ends of the attached tubes are open, the air entering tangentially through D escapes with a screw-like motion along the wall of the left tube, while the centrifugal force and the internal friction of the gas produce a lower pressure in the axial region. Hence, air will be sucked in through B from the right tube. This can be avoided if the flow through the left tube is throttled by a valve attached to the end of this tube. This valve should be sufficiently far away from the nozzle D (about 50 R) so that the gas reaching it will have lost most of its screw-like motion because of internal friction. By partial closing of the valve, it is possible to force a fraction, μ, of the air stream to escape to the right through the diaphragm B. This fraction increases with increasing internal pressure p, which is measured in the left tube near the valve, and it originates in the region near the axis of the vortex in the left part of the tube. The air escaping through B has been expanded in the centrifugal field from a region of high pressure near the wall of the cylinder to a pressure p, in the region near the axis ; and it has transferred a considerable part of its kinetic energy by means of internal friction to the peripheral layers. These flow to the right and acquire a higher temperature. Hence, a fraction μ of the expanded air leaves

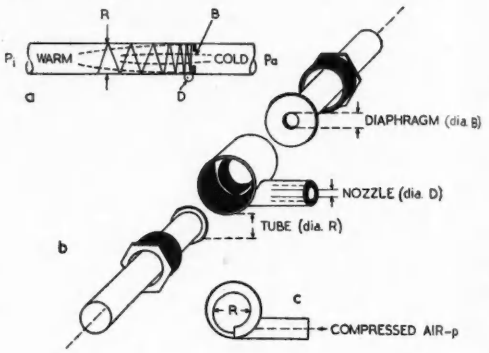

Fig. 1. **Vortex tube.**
(a) schematic sketch ; (b) tube taken apart (thread surfaces black) ; (c) central piece with nozzle.

the tube to the right with reduced temperature, and a fraction $(1 - \mu)$ escapes to the left with increased temperature.

The demonstration of such a vortex tube is simply astonishing. With proper choice of the fraction μ and $1 - \mu$, compressed air of a few atmospheres pressure and 20 deg. C. will easily produce a temperature of + 200 deg. C., in the left tube and — 50 deg. C. in the right tube.

3. DETERMINATION OF THE MOST FAVOURABLE CONDITIONS FOR THE OPERATION OF A VORTEX TUBE.

While the general design is fixed by the simple principles listed above, there are a number of variables to consider which affect the operation. Since it seems rather difficult to derive these influences theoretically from an analysis of the behaviour of the compressible flow in a quantitative form, they were subjected to an experimental investigation. The temperatures of the gas in the two flow directions depend on the following variables :

(1) Temperature, T_0, pressure p ; and rate of flow G of the expanding compressed air.
(2) External pressure p_a outside the vortex tube.
(3) Diameters of the tube (R), the diaphragm (B), and the nozzle (D) ; these quantities determine G.
(4) Ratio of distribution of air between the flow in both directions, μ-mass of cold air/mass of total air.

4. RESULTS.

Fig. 2 contains results obtained with a vortex tube of a diameter $R = 4{\cdot}6$ mm. The effect of the nozzle diameter D cannot be ascertained from this figure, but it was found by experiments that $D = 1{\cdot}1$ mm was a favourable value. Smaller values of D would certainly be less favourable. If they were chosen, the rotating flow would decrease too fast on account of the small rate of flow and the more important contribution of the friction between gas and walls. Larger values of D would result in such large rates of flow that it could not be carried by the tube without increasing the pressure p_i to too large values. This would make

*Scientists have been intrigued by the performance of the "Hilsch tube," so called after a German scientist who did experimental work on it. The thermodynamic phenomena involved were first described by M. G. Ranque (*J. de phys. et rad.* [7], 4, 112, 1933), and the Westinghouse Research Laboratories of America recently conducted fundamental research into the principles underlying this new process. (*Westinghouse Engineer*, July, 1947, pp. 108-109). Commercial applications are being investigated in Great Britain.—Editor, E.D.

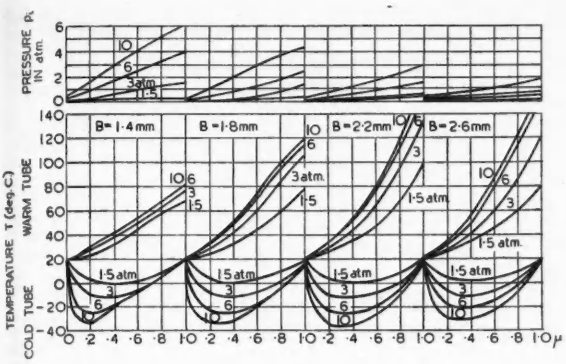

Fig. 2. **Temperature of cold and hot gas stream and internal pressure in tube No. 1 as function of external pressure, size of diaphragm, and μ.** (μ = mass of cold mass of total air.)
Constants: R=4·6 mm, D=1·1 mm, T_0=20 deg. C., p_a = 1 atmos. Parameter: pressure p at the nozzle.

the expansion ratio p/p_i unfavourable. The pressure difference $p_i - p_a$, moreover, causes losses at the throttle.

Fig. 2 shows the temperatures of the cold and warm tubes as functions of μ for four different values of the initial gas pressure p. The ratio μ can be changed by means of a valve attached to the free end of the warm tube, which was about 30 cm long. At such a distance from the nozzle, the rotating component of the gas motion had decreased sufficiently. The value of μ was measured with two gas meters arranged in the cold and warm stream, respectively. The total rate of flow is proportional to the absolute pressure p of the entering gas, but is practically independent of the setting of the valve and, therefore, of μ. For D = 1·1 mm and air, the rate of flow was, for instance, G = 7·0 m³/hr. for p = 10-atmos. gauge pressure. The internal pressure p_i was measured near the throttle valve and is also plotted in Fig. 2. The influence of the diameter of the diaphragm B is shown for four different values.

There is always a certain value of μ producing a minimum value of the temperature of the cold air. The larger the value of μ, the higher the temperature of the warm end. A small diaphragm (B = 1·4 mm) is rather unfavourable, especially at high values of μ, since then the internal pressure p_i and the throttle losses become too large. On the other hand, the largest diaphragm (B = 2·7 mm) gives a smaller cooling effect in the minimum of the curve because it permits the entrance of air from regions where the rotating flow is still considerable. For large values of μ (e.g., 0·8), the most favourable cooling effect is obtained with the largest diaphragm. The choice of the diaphragm diameter B depends, consequently, on whether it is desired to reach very low temperatures or to produce large quantities of cold air. The value B = 2·2 mm may be considered as a most favourable compromise solution for these two factors.

Many more details may be seen in the curves. It should be pointed out, in particular, that the cooling of the cold air and the heating of the warm air with respect to room temperature are equal for μ = 0·5. It is easy to see, moreover, that the relation

$$\mu \text{ (cooling)} = (1 - \mu) \text{ (heating)}$$

must always be valid since the amount of heat removed from the cooled air must be equal to the amount of heat given to the heated air. It should also be remarked that the setting of the throttle valve giving minimum temperature can be found easily without special measurements; a boiling sound is audible if the valve is set for the correct value μ (e.g., μ = 0·3 for 10 atmos. and B = 2·2 mm, T = — 35 deg. C.). It should be realized that the temperature of the cold air is measured too high if μ is very small, and the temperature of the warm air is measured too low if μ is near 1, because in both cases the rate of flow through the tube in question is very small.

It would be necessary to repeat all the measurements for different values of the tube diameter R, in order to investigate the influence of this quantity. It is, however, sufficient to report the measurements in the cold air stream with the most favourable value of the diameter of the diaphragm B for a wider tube (Fig. 3). The diameter of the tube R has been increased to more than twice its former value, and the nozzle diameter D in proportion. In this case, the temperatures of the cold air are lower than those in Fig. 2 for all values of p. Additional data for the lowest temperatures obtained with a still larger tube as function of p are given in Fig. 4. The total rate of flow G for all tubes may be represented by the relation

$$G = \text{const.} \times F \times p,$$

where F is the area of the nozzle in mm², p the initial

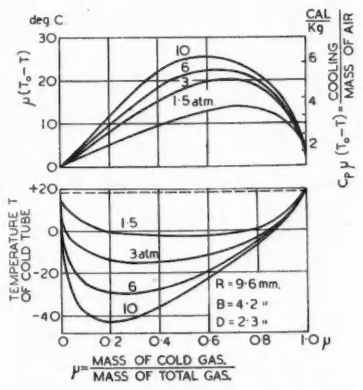

Fig. 3. **Temperature and heat content of the cold air stream of tube No. 2 with most favourable diaphragm.**

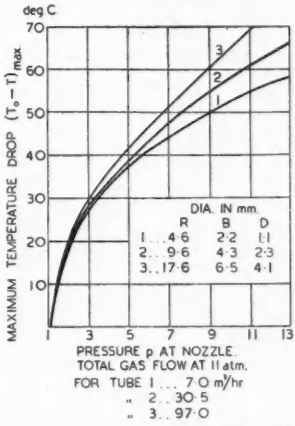
deg C
MAXIMUM TEMPERATURE DROP $(T_0 - T)_{max}$
DIA. IN mm.
R B D
1 . . 4·6 2·2 1·1
2 . . 9·6 4·3 2·3
3 . . 17·6 6·5 4·1
PRESSURE p AT NOZZLE
TOTAL GAS FLOW AT 11 atm.
FOR TUBE 1 . . . 7·0 m³/hr
" 2 . . 30·5
" 3 . . 97·0

Fig. 4. **Maximum temperature drop for tubes Nos. 1, 2, and 3.**

air pressure in atmos., G the rate of air flow in kg/hr., and const. = 0·80 kg/(h mm² atmos.).

Finally, we show in Fig. 3 the product $\mu(T_0 - T)$ as function of μ for tube No. 2. This product is proportional to the total cooling effect. It is apparent that the maximum heat removal does not occur at the value of μ for which the lowest temperature is obtained.

It follows from Fig. 4 that increasingly larger temperature reductions and cooling effects may be obtained with larger vortex tubes at the same initial pressure. The rates of flow, however, become considerable and the capacity of the compressor which was available did not permit the use of larger tubes.

5. THERMODYNAMIC EFFICIENCY OF A VORTEX TUBE.

The calculation of the cooling efficiency of a vortex tube will be carried out by comparing it with the cooling efficiency of the adiabatic expansion of a perfect gas in an expansion engine delivering external work. Such an engine will, theoretically, deliver a continuous flow of cold air of the temperature T_1, produced by expanding a gas of the temperature T_0 from the pressure p to the pressure p_a. For this process,

$$T_0/T_1 = (p/p_a)^{(\gamma-1)/\gamma} \quad .. \quad .. \quad (1)$$

The work E delivered by the expansion engine per unit mass is $E = c_p\,(T_0 - T_1)$ and is equivalent to the amount of heat Q removed from the gas. The minimum amount of work required for (isothermal) compression is

$$A = RT_0 \log_e \frac{p}{p_a} \quad .. \quad .. \quad .. \quad (2)$$

Substituting for p/p_a from eq. (1), one obtains

$$A = c_p T_0 \log_e \frac{T_0}{T_1} \quad .. \quad .. \quad .. \quad (3)$$

The net work required is $A - E$, and the result obtained for the efficiency of the expansion engine is

$$\eta_E = \frac{Q}{A-E} = \frac{T_0 - T_1}{T_0 \log_e (T_0/T_1) - (T_0 - T_1)} = \frac{x-1}{x \log_e x - (x-1)}, \quad (4)$$

where $x = T_0/T_1$.

The efficiency of the vortex tube is less than that of the expansion engine, since only a fraction μ of the gas is expanded into a cold stream and heat is removed by another fraction of the gas $(1-\mu)$. Moreover, no expansion work is gained.

The efficiency of an ideal vortex tube would be larger than that of a real vortex tube, since almost all the gas would escape as a cold stream through the diaphragm. No expansion work would be developed in this case ; its heat equivalent would be carried off by the minute amount of gas escaping through the warm tube. The efficiency of such an ideal vortex tube shall be compared with that of the actual vortex tube ; it is obtained by omitting the expansion work E in the denominator of eq. (4). The result is

$$\eta_W = (x-1)/x \log_e x. \quad .. \quad .. \quad (5)$$

Fig. 5 shows the dependence of η_E and η_W on x, also, and for comparison only, the efficiency of a Carnot engine η_c. While such an engine is not very practical for the production of a continuous stream of cold air of the temperature T_1, it is frequently used in practice for such a purpose. The upper scales in Fig. 5 show the pressure ratio p/p_a for which the temperature ratio T_0/T_1 is reached for mono- and diatomic gases. For $x = 1$, η_c and η_E approach ∞, while all values of η approach zero for large values of x.

The theoretical efficiency of the vortex tube is rather favourable, especially for large pressure ratios where it approaches the value η_E.

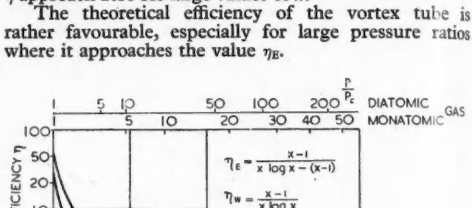

Fig. 5. Efficiency of 3 refrigerating machines for comparison.

The results of these theoretical considerations may now be compared with data for actual vortex tubes found by experiment (Table I). The data given in this table refer to the largest tube No. 3 with a diameter $R = 17{\cdot}6$ mm. Data given in line 2 are taken from the curves in Fig. 4. The values for the quantity $[\mu\,(T_0 - T)]_{max}$ in line 5, which is proportional to the amount of cold Q, are taken from the curves in Fig. 3 and have been multiplied with a factor 1·1 (see Fig. 4), in order to obtain corresponding values for tube No. 3. It is apparent that the obtained temperature drop α reaches almost 50 per cent of the theoretical value. The "cooling efficiency" B is defined as the ratio between the actually obtained efficiency and the theoretically calculated efficiency; it amounts to about 20 per cent. The practical thermodynamic efficiency in line 8 is defined as $B\eta_W$; this definition would be valid if an ideal air compressor would be used.

It is probable that the real efficiencies are somewhat better than the data in Table I indicate. This is caused by, firstly the method of temperature measurement which gives unfavourable values, and secondly, to the presence of moisture in the compressed air, which appears in the cold stream as a fog of ice crystals.

TABLE I. Efficiency of Tube No. 3. $R = 17{\cdot}6$ mm, $T_0 = 18$ deg. C., $p_a = 1$ atmos.

1.	Pressure ratio used (p/p_a)	2·5	4	7	11
2.	Maximum temperature drop $(T_0 - T)_{max}$ ..	24° C	36° C	52° C	68° C
3.	Theoretical temperature drop $(T_0 - T_1)$ ..	67° C	95° C	124° C	144° C
4.	Temperature efficiency $\alpha = (T_0 - T)_{max}/(T_0 - T_1)$	0·36	0·38	0·42	0·47
5.	$[\mu\,(T_0 - T)]_{max}$	15·5° C	21° C	24° C	27·5° C
6.	Cooling efficiency $B = [\mu\,(T_0 - T)]_{max}/(T_0 - T_1)$	0·23	0·22	0·19	0·19
7.	Theoretical efficiency η_W	0·88	0·81	0·77	0·72
8.	Practical efficiency $B\eta_W$	0·20	0·17	0·15	0·14

6. APPLICATIONS OF THE VORTEX TUBE.

There is little probability that vortex tubes will replace the customary refrigerating machines, since their efficiencies are much better in the region of small pressure ratios. There may, however, be special cases where a vortex tube would be more desirable because of its simple construction (e.g., air cooling in mine shafts).

The situation is different at low initial temperatures and high pressure ratios. It may be expected that the vortex tube will be superior to the throttle expansion (Joule-Thompson effect) for gas liquefaction.

Apparatus for the Rapid Taking of Magnetization Curves

By K. P. BELOV and G. M. STRAKHOVSKIJ. (From *Zavodskaja Laboratorija*, No. 6, 1946, pp. 577-582, 8 illustrations).

THE increasing importance of the principle of magnetic analysis which can be employed in many ways for the investigation of fundamental properties, deficiencies, etc., of metals has led to the prospective use of the cathode-ray oscillograph for taking magnetization curves or hysteresis loops. It was hoped with good reason, that such method would accelerate and make automatic the process, but the intrinsic difficulties to be overcome in each of the methods so far suggested have as yet prevented their adoption.

The suggestions made can be divided into two groups. In the first, the specimen is placed near the cathode-ray tube, sometimes held in a yoke in the air gap of which the neck of the tube is inserted. The x-deflection is obtained magnetically by a current proportional to the magnetizing current passed through induction coils around the beam, or neck of the tube. However, a substantial drawback of such systems is that owing to the presence of an air gap the loop will be distorted (influence of the demagnetizing factor) and so far this has not been eliminated. The second group comprises arrangements working with a wire or toroidal specimen placed at a distance from the beam, which is deflected by the plates of the tube to which the voltage of a secondary coil is applied, known as " search coil " and wound around the specimen. As this voltage is proportional to $d\Phi/dt$, it must be passed through a special electric integrator to be made proportional to Φ before being applied to the plates. This, however, cannot be effected without substantially reducing the voltage, which must therefore be stepped up again by an amplifier. The x-deflection may be obtained electrostatically or electromagnetically, by a voltage, or current respectively, proportional to the magnetizing current. If the phases of H and Φ coincide, the hysteresis loop will appear on the screen. It is this synchronization which constitutes the main difficulty because the amplifier is indispensable. Apart from the absence of linear and frequency distortion which is absolutely necessary, no phase shift must occur between the amplifier input and output voltages because, even when insignificant in amount this gives a distorted loop, i.e. it renders the hysteresis loop practically useless.

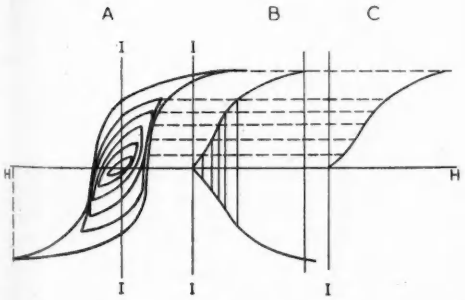

Fig. 1. **Method of obtaining the magnetization curves on the screen of a cathode-ray oscilloscope.**

The method suggested by the authors is based on the following principle :—Assuming that the alternating magnetizing field passes through an ascending series of values, the magnetic induction then will also pass through a corresponding series of values, each of which is characterized by its own particular hysteresis loop (Fig. 1A). The locus of the end points of all these " ascending " loops is known as the initial (" virgin ") magnetization curve (Fig. 1A), and the doubled ordinate of each end point of the loops represents the full amplitude of the flux density corresponding to this particular loop. This amplitude can be obtained on the screen of the oscillograph as a vertical line, if a voltage proportional to the flux density in the material is applied to the y-plates. By shifting this vertical line along the x-axis through a distance proportional to the increase of the magnetizing force, which is done by the x-plates, an uninterrupted sequence of parallels of increasing length can be obtained which thus represent the rising end ordinates of consecutive loops. The curve through the end points of these lines gives two " virgin " curves, one for each the positive and the negative ordinates (Fig. 1B). Using a detector for rectification, the positive (or negative) half of the magnetization curve is obtained as shown in Fig. 1C. The block diagram of the set-up for taking the initial magnetization curves is shown in Fig. 2.

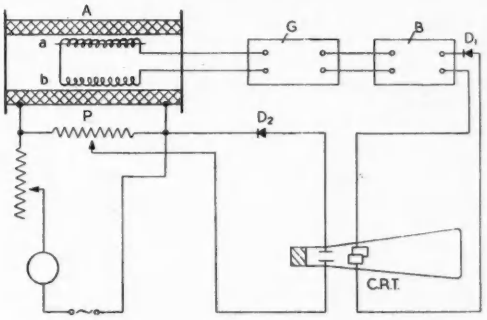

Fig. 2. **Schematic diagram of the installation.**

The specimen is placed inside a magnetizing coil passed by a 50 c.p.s. alternating current. Two identical coils are connected in opposition to each other so that the e.m.f.'s induced in them (proportional to $d\Phi/dt$) exactly balance each other. Yet when a ferromagnetic specimen is introduced into one of the coils, then an e.m.f. is set up in the circuit of the two coils which may be written :—

$$E_2 - E_1 = K\frac{dI}{dt}$$

where I is the magnetization of the tested specimen, and K is a constant. The numerical value of K is obtained from the elementary relation

$$K = 4\pi n S \cdot 10^{-8}$$

where n is the number of turns, and S is the area of the cross-section of the specimen.

By means of a resistance and a condenser, dI/dt may be integrated electrically, so that an e.m.f. proportional to I is obtained. Indeed, if the current set up in the coils a and b is fed into a series circuit consisting of a capacitance C and a resistance R, we have the relation

$$E_2 - E_1 = K\frac{dI}{dt} = iR + \frac{1}{\omega C}i$$

Now assuming $1/\omega C$ to be negligible compared with R,

$$K \frac{dI}{dt} = i R$$

and the potential difference across the condenser becomes

$$V_c = \frac{K}{RC} \int \frac{dI}{dt} dt = \frac{K}{RC} I$$

After amplification, the potential difference V_c is applied to the y-plates of the oscillograph and on the screen a vertical line proportional to I is obtained. The horizontal shift is obtained in the following way :— A large resistance, P, is shunted across the magnetizing circuit, and the voltage across the latter, after rectification in the detector, D_2, is applied to the x-plates. It is evident that the increases of this voltage are proportional to those of the magnetizing field. Thus the shift may be photographed or traced from the screen. The numerical value of I is obtained as follows :

The oscillograph is initially calibrated by feeding into the amplifier a voltage of known amplitude. Let 1 volt cause a deflection of the trace on the screen of e cm. Then if the voltage V_c fed to the amplifier gives a deflection α, the magnitude of V is known.

Now

$$V_c = \frac{4 \pi n S \times 10^{-8}}{RC} I = \frac{\alpha}{e}$$

and consequently $$I = C' \alpha$$

where $$C' = \frac{RC \times 10^8}{4 \pi n S e}$$

The flux density is determined as follows :

As the resistance P is shunted across the magnetizing coil, the peak voltage V, tapped off from this resistance and applied to the plates of the oscillograph is

$$V = i \sqrt{r^2 + \omega^2 L^2}$$

where r, L, and i are resistance and inductivity of the magnetizing coil, and magnetizing current, respectively. If :

$$H = Ki$$

where K is the constant of the coil, and $V = e_1 \beta$, e_1 representing the electrostatic sensitivity of the oscillograph, and β the deflection of the trace on the screen, we get

$$H = \frac{K e_1}{\sqrt{r^2 + \omega^2 L^2}} \beta$$

Owing to the small dimensions of the specimen, the inductivity L may safely be assumed to remain constant against changes of the magnetizing current. Practical work with the apparatus showed that it is sometimes convenient to calibrate by parallel measurements with the usual ballistic galvanometer circuit for taking magnetization curves, which may easily be done simultaneously. This is possible because for small specimens the distortions of the magnetization curve owing to Foucault currents are negligible. Fig. 3 shows the actual circuit diagram, on which A is the magnetizing coil, G is the electrical integrator, B is the amplifier, with the detector D_1, P is the potentiometer shunt with the second detector, D_2, and the oscillograph is C.R.T. In order to keep the influence of the demagnetizing factor as small as possible, the specimen is in a form with as large as possible a ratio of length to diameter, which calls for a very long and narrow magnetizing coil, to ensure maximum homogeneity of the field. Furthermore, the small cross-section of the specimen allows the mutual induction between search coil and magnetizing coil in its effect on the inductivity of the latter and, finally, the magnetic skin effect on the magnetizing curves to be neglected. An indispensable condition for correct electrical integration is

$$\frac{1}{\omega C} < 0{\cdot}02\, R$$

because in the integrating circuit the condenser is in parallel with its own leakage resistance, and with the leakage resistance of the first valve of the amplifier, it is necessary to select a condenser with a big leakage resistance. The leakage resistance of the first valve should be large compared with the impedance of the condenser. As for freedom from linear and phase distortion of the amplifier, it should be remembered that, as in the present case only the magnitude of the amplitude is recorded on the screen, this requirement is no longer important provided there is no overcrowding of frequencies around 50 c.p.s. This means that any commercial amplifier may be used.

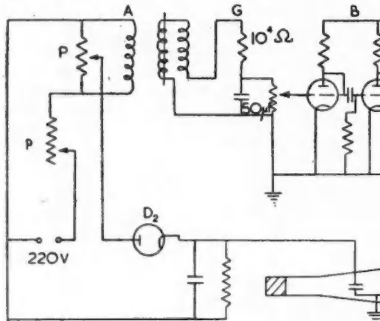

Fig. 3. **Actual circuit diagram.**

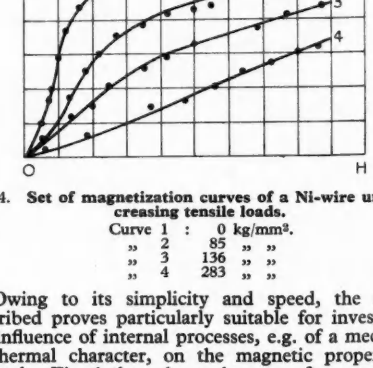

Fig. 4. **Set of magnetization curves of a Ni-wire under increasing tensile loads.**

Curve	1	: 0	kg/mm².
»	2	85	» »
»	3	136	» »
»	4	283	» »

Owing to its simplicity and speed, the method described proves particularly suitable for investigating the influence of internal processes, e.g. of a mechanical or thermal character, on the magnetic properties of a metal. Fig. 4 thus shows, by way of an example, a family of magnetization curves of a Nickel wire, which has negative magnetostriction. Accordingly, it is seen that the curves straighten out progressively as the tensile load on the wire is increased, so that under the maximum tensile stress (283 kg/mm²) a practically straight line is obtained. Fig. 5 gives a particularly striking example of the differential method of measurement applied to the investigation of the effect of elastic stresses on the magnetic characteristics. This method consists in first placing the specimen in coil a, and then in coil b, when the curves 1 and 2, respectively, are

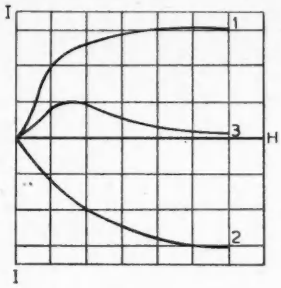

Fig. 5. **Example of the differential measuring method.**

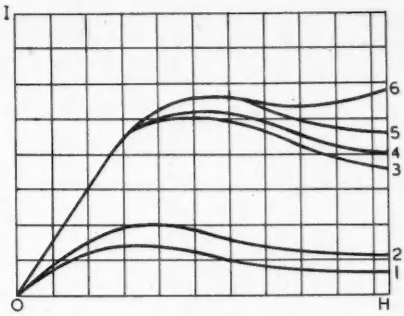

Fig. 6. **Magnetization curves of carbon steel rods tempered at different temperatures.**

Curve	1	750 deg. C.
"	2	790 "
"	3	830 "
"	4	870 "
"	5	910 "
"	6	95 "

obtained. Curve 3 results when two specimens of the same material are simultaneously placed in the coils *a* and *b*, and thus reveals the deviations of a chosen specimen from a standard specimen. By increasing the amplification a substantial increase in the sensitivity of this method is possible. It should be noted that the curves shown were obtained in a few minutes, whilst to take them by the conventional ballistic method would have required several days' work. Eventually, Fig. 6 shows an example of the application of this method in the control of the tempering of carbon steel at different temperatures, with an untempered steel rod serving as a standard. It should be stressed that the measurements may be carried out at any desired temperature.

FRANCE

Fractographic Studies of Ferro-Chromium Alloys

By C. A. ZAPFFE. (From *Revue de Métallurgie*, Vol. 44, No. 3/4, March/April, 1947, pp. 91-96, 17 illustrations.)

FRACTOGRAPHY, developed just before the war, is the study, by microscopic enlargement, of unpolished and unetched cleavage planes in the fracture face of a metal. The sample is mounted on an adjustable tripod or on a special fractographic slide developed by Bausch and Lomb, and a chosen crystal facet is adjusted to be normal to the incident light. Réaumur and Martens began this study but were discouraged by the difficulty of obtaining flat fracture surfaces. Therefore the conventional technique of polishing and etching was developed. Fractography, however, is particularly interesting because (1) it allows for the observation of special constitutional structures new to metallurgy, and (2) it furnishes direct and repeated proof that the mosaic structure is an intrinsic property of all crystalline matter, especially metals.

Samples weighing about 4·5 lbs. were obtained from electrolytic iron and commercial low-carbon ferro-chromium, mixed in an induction furnace, and cast in rectangular moulds. The chemical analyses are given in Table I. All samples were homogenized-annealed for 40 hours at 875 deg. C., and then cooled in air. For some of the alloys referred to in Table I, i.e., those corresponding to commercial stainless steel alloys, this temperature is above the usual annealing temperature but below the required quench temperature. In fact, no sample was completely hardened by this treatment. In some cases, therefore, duplicate samples were heated 15 minutes at 980 deg. C. and quenched in oil so that the influence of heat treatment on the cleavage figure could be studied.

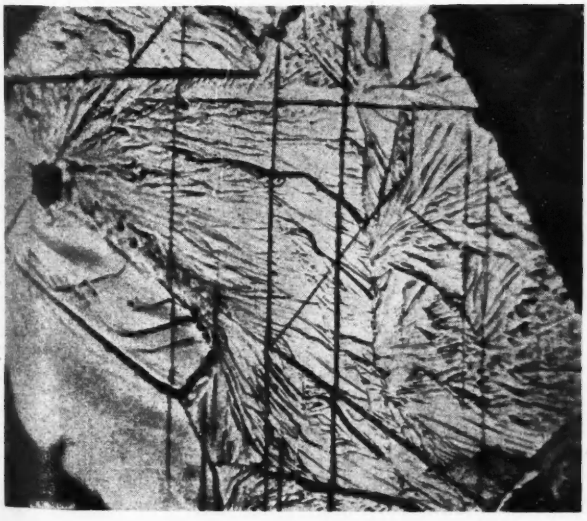

Fig. 1. **Fractograph of re-molten electrolytic iron, broken by impact at liquid air temperature, showing Neumann bands and other structural design. ×500 (reduced to abt. 1/6 by reproduction).**

Fig. 1 shows the fracture of molten and cast unalloyed electrolytic iron broken by impact after immersion in liquid air so that a brittle fracture was obtained. Neumann bands are visible at angles of 90, 45, 60, and 30 deg. to each other and to the cleavage structure of the grain. Other crystallographic and non-crystallographic markings are also observed but some are unexplained. Perhaps the undulating lines represent the much discussed primitive

Fig. 2. **Fractograph of fluor spar crystal showing structure of structural weakness comparable to that of Fig. 1.**

Fig. 3. **Fractograph of 7·70 per cent chromium alloy, air cooled from 875 deg. C., showing oak leaf design associated with martensitic structure and tough materials.**

(Fig. 3) and large crystallographic marks are absent. Only when greatly magnified can undulating and irregular markings be seen to follow small crystallographic

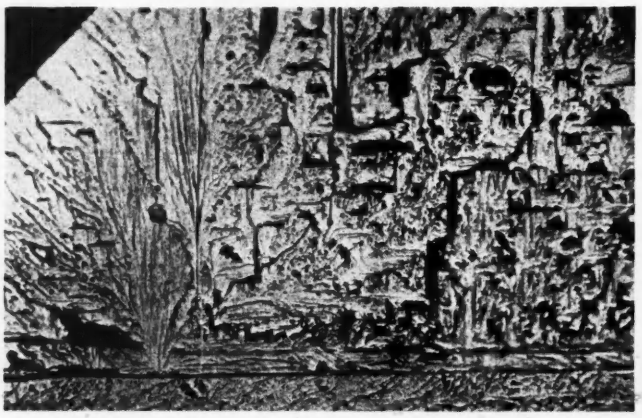

Fig. 4. **Fractograph of Alloy IV showing typical rectangular cleavage design of ferrite and an anomaly in the form of primitive growth at one side.**

Fig. 5. **Fractograph of 17·16 per cent Cr alloy, air-cooled from 875 deg. C., showing strongly developed cleavage facets of rectangular, ferritic design and leaf structure considerably different from the martensitic structure.**

structure. In any case, there must be some signs of the brittleness which led to the fracture.

Fluor spar (Fig. 2) shows no Neumann bands but there are crystallographic and non-crystallographic markings resembling those of iron, and this structure is evidently associated with fluor spar brittleness. The strength of metals is only a small proportion of the strength of perfect crystals, and the difference must be due to internal imperfections which probably show up on these photographs and can be studied by comparing different structures. Eliminations of these inperfections would increase the strength of metals enormously.

Additions of less than 12 to 14 per cent chromium produce martensitic steels known for strength and toughness. The small fracture facets therefore do not show the regularity of cleavage patterns and are difficult to observe. "Oak leaf" facets are formed

TABLE I.

Chemical analysis of samples (weight per cent).

Alloy No.	Chromium	Carbon	Other elements
Electrolytic iron :			
I	7·70	0·102	—
II	12·58	0·096	—
III	14·85	0·075	—
IV	14·29	0·047	—
V	17·16	0·103	0·23 *Al*
VI	22·14	0·096	—
VII	28·67	0·107	—

steps, thus confirming the conception of a mosaic structure. This structure can provisionally be attributed to martensite, although it is possible that martensitic stresses produce this figure in neighbouring phases since heat treatment at 875 deg. C. takes place very near the A_3 point. A duplicate sample of Alloy II was heat treated and quenched but the fracture facets were so small and severely twisted that no clear photograph could be taken.

With nearly 15 per cent chromium, isolated facets appear showing a neat crystalline cleavage pattern (Fig. 4). Note the rectangular character of the facets, the mosaic structure, and the dendrites or inter-crystalline junctions at exactly 45 deg. to the cleavage planes. Because the metal fractures along cleavage planes, the fractographs show the orientation of the single crystal. It is practically certain that Fig. 4 shows one crystal only, and the junctions at 45 deg. must therefore represent a structural feature inside the crystal. Due to the addition of 0·25 Al, the sample of Alloy IV was predominantly ferritic ; it was taken from a commercial steel showing surface decarburization in an etched specimen, and was broken after hot rolling. Fig. 4 is thus characteristic of ferrite. The cleavage marks

Fig. 6. **Conventionally polished and etched cross-section of Alloy V, oil-quenched from 980 deg. C. showing rather equal distribution of ferrite and martensite.**

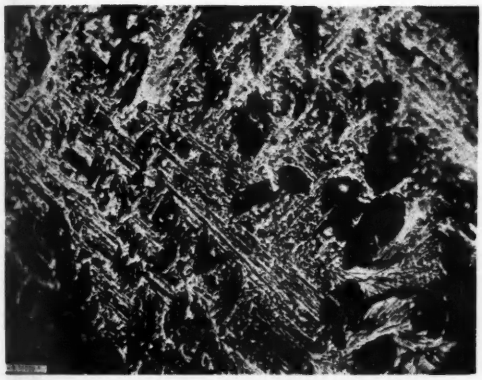

Fig. 7. **Fractograph of sample of Fig. 6. Rectangular cleavage design of ferrite with large hollows where tough martensite has broken out on fracture.**

Fig. 9. **Conventionally polished and etched section of Alloy VI, oil-quenched from 980 deg. C., showing partial re-dissolution of carbides.**

extend comparatively without interruption showing the lack of strength of ferrite. Numerous big hollows are without doubt, due to martensite particles broken out by fracture from the softer ferrite matrix. The ramified structure at one side of Fig. 4 shows a leaf pattern very different from that of martensite (Fig. 3) and is probably due to some defective growth, perhaps a primitive structure. Even in this, metal has been broken out in geometrical shapes confirming the mosaic structure theory.

Alloy V corresponds to an important commercial alloy. The chromium content is so high that a great part of the structure remains ferritic even above the austenitic transformation point. These alloys are only slightly hardenable, and treatment at 875 deg. C. can only give a reduced quench. Fractographs show (Fig. 5) (1) large plane facets typical of a structure lacking toughness, i.e. ferrite predominates ; (2) a leaf structure, superimposed on the rectangular ferritic structure, giving the impression of an intermediate structure between martensite (Fig. 3) and ferrite (Fig. 4) ; (3) that the leaf pattern does not prevent the general extension of cleavage planes characteristic of low strength ; and (4) that the leaf design has changed its direction by 90 deg. at several places, which is further proof of the mosaic theory.

A duplicate specimen, oil-quenched from 980 deg. C. shows the conventional metallographic structure of

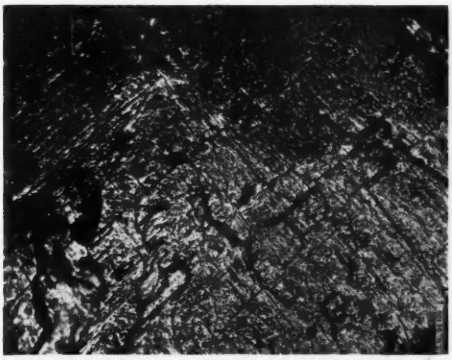

Fig. 8. **Fractograph of 22·14 Cr alloy, air-cooled from 875 deg. C., showing typically ferritic rectangular cleavage design and a perfect substructure of primitive growths and mosaic blocks.**

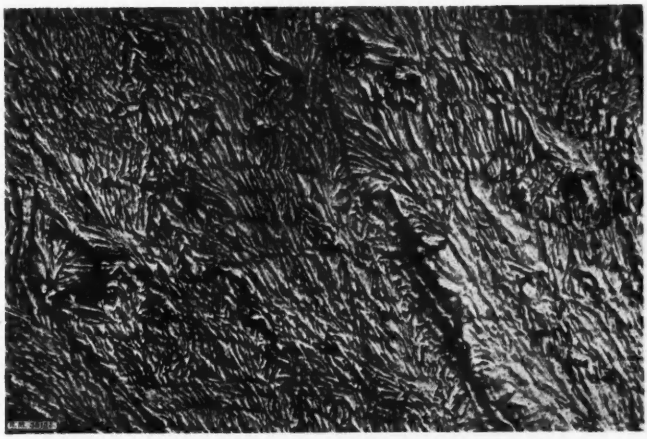

Fig. 10. **Fractograph of Alloy VI, oil-quenched from 980 deg. C., showing completely modified ferritic structure.**

Fig. 6, partly ferritic, and partly martensitic. Fig. 7 shows a typically ferritic fractographic structure with large hollows where martensitic particles have broken out on fracture. Primitive growths can be seen especially in the bottom right hand corner and suggest a possible relationship with the martensitic structure. Crystal distortion by impurities is probably the common origin of both.

With 22 per cent chromium, the alloy is completely ferritic and shows characteristic cleavage marks at 90 deg. and, occasionally, traces at exactly 45 deg. The facet structure is very fine and contains numerous very small imperfections according to the mosaic theory. Very small primitive growths and block structures, of a few microns extension, are certainly the cause of the special mechanical properties of this alloy (Fig. 8). After an oil-quench from 680 deg. C., conventional micrography shows a partial redissolution of the carbides, and the fractograph shows a remarkable change of the cleavage design (Figs. 9 and 10). No explanation can be put forward but the undulating lines resemble the "rifflemarks" observed in bismuth[2,6] and in a Fe-Si alloy[3] and afford further evidence that the cleavage structure gives a sensitive indication of metallurgical changes in the crystal.

Commercial stainless steel with 28 per cent chromium shows large ferrite grains and finely dispersed carbides in etched specimens. Fig. 11 shows extensive cleavage planes of rectangular ferrite, with or without primitive growths, which do not break the cleavage planes, however, as the matensite does. Grain boundaries and mosaic detail can be clearly seen. Fig. 12 exemplifies two main points of the present investigation ; (1) the cleavage figures clearly show the characteristics of different phases which can be easily interpreted once the fractographic figures are as well understood as micrographic features are understood to-day, ; (2) cleavage figures show an abundance of small structural details within the grain which cannot be discovered by conventional methods. Note the uninterrupted cleavage of Fig. 11, explaining the mechanical weakness of the material, the mosaic detail, and the interesting junction in Fig. 12. This junction is not a grain boundary because crystallographic orientation passes across it without noticeable change of direction.

The endurance and fatigue of metals are certainly affected by imperfections revealed in fractographic studies. Theories of the distortion of perfect lattices cannot correspond to facts when obvious faults are so much more influential in producing the explicit cleavage pattern. The internal surfaces thus revealed must be characteristic of each metal constitution, otherwise the fracture patterns would not be so regular and reproducible for each separate phase as well as for changes of conditions with one phase.

Toughness is probably the most important mechanical property and the most difficult to define clearly. Tensile strength, ductility, and impact resistance are only indirect and inadequate expressions of this characteristic. However, it seems to be directly observable in fractographs and the fractographic technique thus offers interesting possibilities in being directly applicable to the evaluation of metal toughness.

BIBLIOGRAPHY.

(1) ZAPFFE & MOORE, *Micrographic cleavage study of hydrogenized ferrite, Metals Techn.* **10**, No. 2, T.P. 1553, 1943, *Trans. Am. Inst. Min. Met. Eng.*, **154** *p.* 335, 1943.

(2) ZAPFFE & CLOGG, *Fractography, a new metall. technique, Trans. Am. Soc. Metals*, **34**, *p.* 71, 1945. *Steel*, 116, No. 22, *p.* 106, 150, 1945.

(3) ZAPFFE & CLOGG. *Cleavage structures in Fe-Si alloys, Trans. Am. Soc. Metals* **34**, *p.* 108, 1945.

(4) ZAPFFE, *Dissociation reactions in inclusions. Preprint*, 1946, *Iron & Steel Inst.*

(5) ZAPFFE, *Neumann bands and the theory of face pressure by hydrogen embrittlement. Preprint*, 1946, *Iron & Steel Inst.*

(6) ZAPFFE, *Fractographic studies in bismuth. To appear in Metal Progress.*

(7) ZAPFFE, *Fractographic studies in zinc. To appear in Metal Progress.*

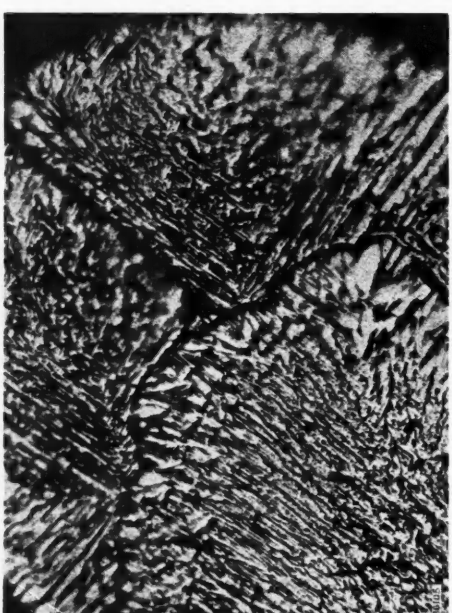

Fig. 11. **Fractograph of Alloy VII showing typical ferritic cleavage structure in an aggregate of several grains.**

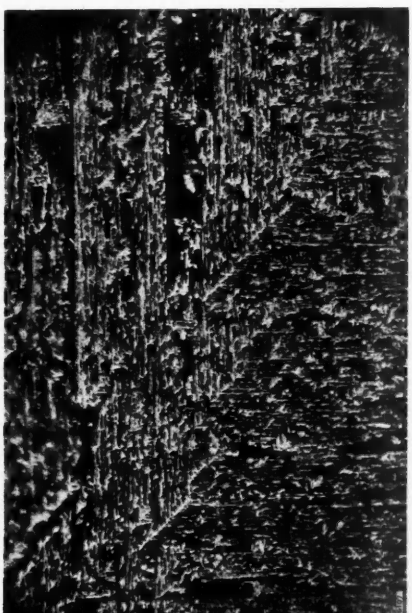

Fig. 12. **Fractograph of the alloy of Fig. 11 showing an intercrystalline dendrite-like, junction and abundant mosaic detail.**

Dimensioning Permanent Magnets

By W. JANSSEN. (From *Hasler-Mitteilungen*, Vol. 6, No. 2, August, 1947, pp. 38-48, 12 illustrations.)

THE object of this article is to investigate the principles involved in the dimensioning of magnetic systems and to review the work which has been accomplished in this field.

1. BASIC EQUATIONS FOR THE DIMENSIONING OF STATIC MAGNETIC SYSTEMS.

In the absence of electric fields and currents, a magnetic field **H** can be defined by curl **H** = 0, or using Stokes's theorem, by $\oint \mathbf{dsH} = 0$, the line integral being taken along any closed path **s**. The non-vorticity of the field **H** can also be expressed by means of a scaler magnetic potential $V = \int \mathbf{dsH}$.

The difference in magnetic potential, V_{ij}, between two surfaces F_i and F_j is obtained by integrating this expression along the field line s_{ij} :

$$V_j - V_i \equiv V_{ij} = \int_{F_i}^{F_j} ds_{ij}\, H \quad .. \quad .. \quad (1)$$

where H is tangential to the line element ds_{ij}. Furthermore, the magnetic induction is given by $B = \mu(s) \,.\, H(s)$, where μ is the (variable) permeability of the medium.

By assuming that there is a tube of flux, of cross-section df_{ij}, around each element ds_{ij} of the field line s_{ij} we can put

$$d\Phi_{ij} = B df_{ij} = \text{const.},$$

the magnetic flux $d\Phi_{ij}$ being regarded as constant within the infinitesimal tube of flux. Hence eq. (1) can be re-written as follows :

$$V_{ij} = \int_{F_i}^{F_j} ds_{ij} \frac{B df_{ij}}{df_{ij}} = d\Phi_{ij} \int_{F_i}^{F_j} \frac{ds_{ij}}{df_{ij}} \quad .. \quad (2)$$

Furthermore, if the reluctance is defined by

$$\frac{1}{dP_{ij}} = \int_{F_i}^{F_j} \frac{ds_{ij}}{df_{ij}} \quad .. \quad .. \quad (3)$$

then $V_{ij} = d\Phi_{ij}/dP_{ij}$ and eq. (2) becomes

$$d\Phi_{ij} = V_{ij}\, dP_{ij} \quad .. \quad .. \quad (2')$$

and the integral over the entire cross-section of the flux gives

$$\Phi_{ij} = V_{ij}\, P_{ij} \quad .. \quad .. \quad (4)$$

This equation is the magnetic equivalent of Ohm's law in the theory of electric currents. It states that the magnetic flux between two equipotential surfaces F_i and F_j is equal to the product of the difference in magnetic potential and the permeance, or magnetic conductance, of the intermediate space.

The total flux Φ of the magnetic circuit is then

$$\Phi = \sum_{(ij)} V_{ij}\, P_{ij} \quad .. \quad .. \quad .. \quad (5)$$

where $\sum_{(ij)}$ represents the sum of all the products of V_{ij} and P_{ij} occurring between two equipotential surfaces F_i and F_j.

In a well-designed magnetic circuit the end faces of the magnet are generally separated from the surrounding medium by pole pieces which have a permeability $\mu \gg 1$. The free faces of the pole pieces can then be regarded as equipotential surfaces ; their differences in potential are approximately equal, and shall be denoted by V_a.

In this case eq. (5) becomes

$$\Phi = V_a \sum_{(ij)} P_{ij} = V_a P \quad .. \quad .. \quad (6)$$

where P is the total permeance of the magnetic circuit. Then, because the field H is irrotational,

$$\oint ds H = \int_{\text{magnet}} ds H + \int_{\substack{\text{external} \\ \text{space}}} ds H = V_m + V_a = 0$$

from which it follows that $V_m = -V_a$ .. .. (7)

If l_m is the mean length of the magnet, F_m its mean cross-section, H_m the mean intensity of its magnetic field, and B_m the corresponding induction, or flux density, then

$$V_m = H_m l_m \quad .. \quad .. \quad (8)$$

and $$\Phi = B_m F_m \quad .. \quad .. \quad (9)$$

so that eq. (6) can be re-written as

$$B_m F_m = -H_m l_m P$$

and on introducing the quantity $p = -B_m/H_m$, we have

$$p = -\frac{B_m}{H_m} = \frac{l_m P}{F_m} \quad .. \quad .. \quad (10)$$

The multiplication of eq. (8) by eq. (9) gives an expression for the magnetic energy :

$$\Phi V_m = B_m H_m \,.\, l_m F_m \quad .. \quad (11)$$

Eqs. (10) and (11) are the basic equations for the dimensioning of magnetic circuits. For any circuit, the working point (H_m, B_m) on the demagnetization curve c of the corresponding magnetic alloy can be found from eq. (10) as the point of intersection of curve c with the straight line $B = -pH$ (see Fig. 1). $p = (l_m/F_m)\, P$ is known as the specific permeance, and is defined by eqs. (3) and (10). The demagnetization curve is that portion of the hysteresis loop which appears in the second quadrant ($-H$, B).

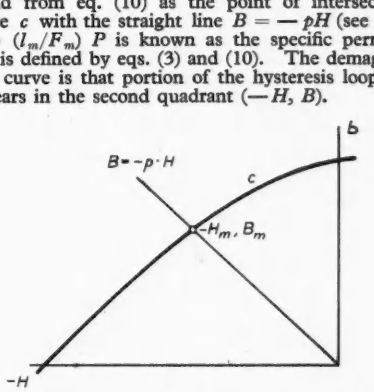

Fig. 1. Determination of the working point of the magnet as the intersection of the demagnetization curve c with the straight line $B = -pH$.

Eq. (11) states that for a given volume of magnet material, the product of the magnetic flux Φ and the magnetic potential difference, or magnetomotive force, V_m,—which is equal to the magnetic energy which the magnet is sustaining in the external circuit—will be a maximum when the product $H_m B_m$ reaches its maximum value. In the case of a normal demagnetization curve (as shown in Fig. 2), the existence of such a maximum is evident. As the energy density HB vanishes

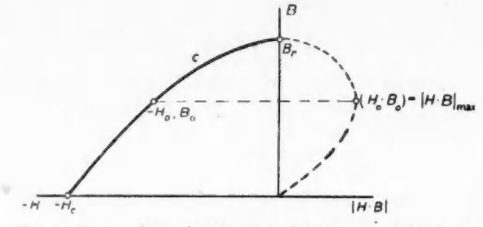

Fig. 2. **Demagnetization curve and optimum working point of a permanent magnet.**

when $H = 0$ and when $H = -H_c$, whilst between these two limits it has a negative but finite value, (HB) must have a maximum within this interval. If the co-ordinates of this maximum are denoted by ($-H_0$, B_0), then

$$| HB |_{max} = H_0 B_0 \quad .. \quad .. \quad (12)$$

2. Analytical Representation of the Normal Demagnetization Curve.

According to E. Watson[1] the demagnetization curve of any type of magnetic alloy can be represented with sufficient accuracy in the second quadrant of the H-B plane by a hyperbolic equation of the form

$$c_1 HB + c_2 B + c_3 H + c_4 = 0 \quad .. \quad (13)$$

Eq. (13) can be divided by any number $\neq 0$ without altering the representation of the curve ; therefore, let

$$c_4 = H_c B_r \quad .. \quad .. \quad (14)$$

where H_c is the coercive force, and B_r the residual magnetization of the alloy.

Instead of working with negative quantities it is more convenient to replace H by $-H$ in the H-B plane, so that the demagnetization curve in the second quadrant will correspond to positive values of H.

When $B = 0$, $H = H_c$, therefore eq. (13) becomes

$$c_3 H_c + H_c B_r = 0,$$

hence $$c_3 = -B_r \quad .. \quad .. \quad (15)$$

When $H = 0$, $B = B_r$, hence eq. (13) becomes

$$c_2 B_r + H_c B_r = 0$$

or $$c_2 = -H_c. \quad .. \quad .. \quad .. \quad (16)$$

Substituting eqs. (15) and (16) in eq. (13) gives

$$c_1 HB + H_c B_r = H_c B + B_r H \quad .. \quad (17)$$

The product (HB) is a maximum at the point (H_0, B_0) on curve c (see Fig. 2), by definition (eq. (12)), so that at this point the variation of (HB) will vanish:

$$d(HB)_{max} = B_0 \, dH + H_0 \, dB = 0, \quad .. \quad (18)$$

therefore

$$\left(\frac{dB}{dH}\right)_{H_0, B_0} = -\frac{B_0}{H_0} \quad .. \quad .. \quad (19)$$

For the differential of eq. (17) at this same point, taking account of eq. (18), we obtain

$$B_r \, dH + H_c \, dB = 0$$

hence

$$\left(\frac{dB}{dH}\right)_{H_0, B_0} = -\frac{B_r}{H_c} \quad .. \quad .. \quad (20)$$

Eqs. (19) and (20) express together the fact that the slope of the tangent to the demagnetization curve at the point of maximum energy-density is also the slope of the straight line connecting the points (H_c, 0) and (0, B_r). The minus sign is because the magnetic field in the magnet has been regarded as positive,

Equating eqs. (19) and (20) gives

$$B_0/B_r = H_0/H_c \quad .. \quad .. \quad (21)$$

This means that on the demagnetization curve of a permanent magnet, the point (H_0, B_0), for which the energy density (HB) is a maximum, can be obtained as the intersection of this curve with the straight line

$$B = \frac{B_r}{H_c} H \quad .. \quad .. \quad (22)$$

For this point eq. (17) becomes

$$c_1 H_0 B_0 + H_c B_r = H_c B_0 + H_0 B_r$$

so that

$$c_1 = \frac{H_c}{H_0} + \frac{B_r}{B_0} - \frac{H_c B_r}{H_0 B_0}$$

As a result of eq. (21), the two first terms on the right-hand side of this latter equation are equal, and hence equal to $\sqrt{H_c B_r / H_0 B_0}$ (since if $a = b$, then $a = b = \sqrt{ab}$), so that finally

$$c_1 = 2\sqrt{\frac{H_c B_r}{H_0 B_0}} - \frac{H_c B_r}{H_0 B_0} \quad .. \quad .. \quad (23)$$

Solving eq. (17) for B gives

$$B = B_r (H_c - H)/(H_c - c_1 H) \quad .. \quad (24)$$

and in conjunction with eq. (23)

$$B = B_r \frac{H_c - H}{H_c - \left[2\sqrt{\frac{H_c B_r}{H_0 B_0}} - \frac{H_c B_r}{H_0 B_0}\right] H} \quad .. \quad (25)$$

Eq. (25) is the analytical expression for the demagnetization curve of a permanent magnet, for the second quadrant of the H-B plane, where H is replaced by $-H$. The following discussion of its properties for two particular types of magnetic circuits is based on the work of D. J. Desmond[2].

3. Magnetic Circuit with Constant Flux and Without Subsequent Demagnetization.

This first case corresponds to conditions occurring for instance with electromagnetic loud-speakers ; it has been extensively investigated by S. Evershed[3]. It will be assumed that the magnet (see Fig. 3) is magnetized after the magnetic circuit has been assembled.

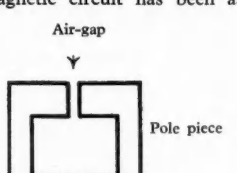

Fig. 3. **Magnetic circuit.**

Generally, a field of about $5 | H_c |$ is necessary for this purpose. The magnetizing equipment is then removed, unless it is an integral part of the completed system. Then the working point A on the demagnetization curve c of the magnet (see Fig. 4) will move away from the point (H, B) = (0, B_r) into the second quadrant of the H-B plane, until the internal field of the magnet has assumed a value which is equal and opposite to that of the original magnetizing field which is determined by the permeances of the working air-gap and the leakage paths.

When considering the design of a magnetic circuit, the problem is usually as follows : To a certain extent, the dimensions of the circuit are already determined, and in particular the mean length l_a and the mean cross-section F_a of the air-gap are given, as well as the mean magnetic flux Φ_a which is required in the air-gap. It is required to determine the minimum volume of the magnet and its dimensions so that the condition regarding the flux may be fulfilled.

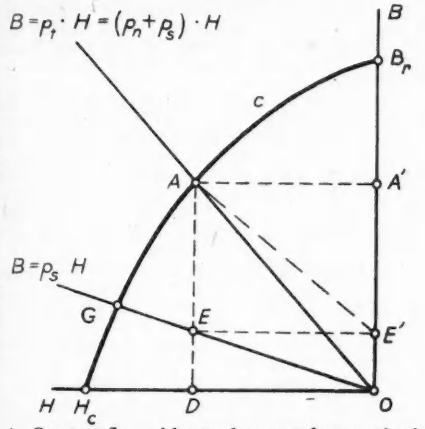

Fig. 4. **Constant flux, without subsequent demagnetization.**

By means of measurements or calculations, or a combination of both methods, the useful permeance P_n and the stray field permeance P_s of the circuit can be determined.*

If it is assumed for the time being that the length l_m and the cross-section F_m of the magnet are known, then, according to eq. (10), the specific permeances p_n and p_s of the circuit can be obtained by multiplying P_n and P_s by l_m/F_m. Using these values, the working point A on the demagnetization curve c can be determined as the intersection of c with the straight line

$$B = (p_n + p_s)\,H = p_t\,H \qquad .. \qquad .. \qquad (26)$$

where p_t is the total specific permeance ($p_t = p_n + p_s$).

From eq. (10) it will be seen that the slope of the straight line defined by eq. (26) will vary when the ratio l_m/F_m of the magnet dimensions is varied. The problem is therefore to determine the optimum value of this ratio in order that there may be an optimum utilization of the magnet material. In other words, it is required to find the optimum working point A_{opt} on curve c.

Considering Fig. 4 again, in this connexion, it will be seen that $\overline{DA}$ represents the total flux per unit volume of the magnet, $\overline{EA}$ the useful flux, and $\overline{DE}$ the stray flux, assuming the magnet has been magnetized homogeneously. Furthermore, the area of the rectangle $AA'OD$ represents the total energy-density stored in the magnet. As according to eq. (11) the energy sustained in the external circuit is equal to the internal energy of the magnet, therefore $\overline{OD}\,.\,\overline{DA}$ is a direct measure of the total energy in the external circuit, which can be divided into a useful energy $\overline{E'E}\,.\,\overline{EA}$ and a stray energy $\overline{OD}\,.\,\overline{DE}$.

Finally the specific permeances p_t, p_n and p_s can be obtained from Fig. 4 as the slopes of the straight lines $0A$, $E'A$ and OG relative to the H-axis.

If the magnetic efficiency η_m is defined as that portion Φ_n of the total flux Φ_t which crosses the working air-gap, we have

$$\eta_m = \frac{\overline{EA}}{\overline{DA}} = \frac{p_n}{p_t} = \frac{P_n}{P_t} \qquad .. \qquad .. \qquad .. \qquad (27)$$

and therefore the useful flux is given by

$$\Phi_n = \eta_m\,\Phi_t \qquad .. \qquad .. \qquad .. \qquad (28)$$

and, also as a result of the above considerations and in conjunction with Fig. 4, the total useful energy is determined by

$$W_n = \eta_m\,W_t \qquad .. \qquad .. \qquad .. \qquad (29)$$

Applying eqs. (7) and (11) to eq. (6), and substituting again $+H$ for $-H$ so as to eliminate the minus sign, we obtain

$$W_t = \Phi_t^2/P_t \qquad .. \qquad .. \qquad .. \qquad (30)$$

P_n and P_s can be determined experimentally or by calculation. Then P_t and η_m are also determined. Provided the dimensions of the magnet are not varied considerably, these four quantities P_n, P_s, P_t and η_m are more or less independent of the magnet dimensions, so that in accordance with eqs. (28) and (30), the useful flux $\Phi_n = \Phi_a$ in the air-gap will be a maximum when the total energy W_t stored in the magnet reaches its maximum value, which is the case when the working point A coincides with the point P_0 (H_c, B_r) of the demagnetization curve c ; $(H_0, B_0) = (HB)_{max}$ applies in this case also. The area of the rectangle $AA'E'E$ in Fig. 4 has a maximum, for if we consider the variation of this area when the optimum working point A is used, and by taking eq. (27) into account, we have :

$$d\,[\overline{E'E}\,.\,\overline{EA}] = d\,[(HB) - (1-\eta_m)\,(HB)]$$

or, since η_m = constant,

$$d\,[\overline{E'E}\,.\,\overline{EA}] = \eta_m\,d\,[(HB)] = 0$$

hence the product (HB) must be a maximum.

The total specific permeance p_t then has a well determined value, obtainable by means of eqs. (21), (22) and (26) :

$$p_{t\,opt} = B_0/H_0 = B_r/H_c \qquad .. \qquad .. \qquad .. \qquad (31)$$

Furthermore, p_s should be made as small as possible. As the magnet dimensions are of finite magnitude, p_s cannot be reduced beyond certain limits.

The optimum ratio of the mean cross-section F_m to the mean length l_m of the magnet, can be obtained from eqs. (10), (21), and (31) :

$$(F_m/l_m)_{opt} = (H_m/B_m)\,P_{t\,opt} = H_0\,P_t/B_0 = \\ = H_c\,P_t/B_r \qquad (32)$$

The total energy of the magnet is given by eq. (30), and is equal to the energy-density (HB) multiplied by the volume $l_m\,F_m$ of the magnet. For optimum utilization of the magnet, its volume must be determined by eq. (30), so that :

$$(F_m\,l_m)_{min} = \Phi_t^2/[P_t\,(HB)_{max}] \qquad .. \qquad .. \qquad (33)$$

As a rule, the value of the useful flux Φ_n, and not that of the total flux, Φ_t, is prescribed. With the aid of eqs. (27) and (28), eq. (34) can be transformed as follows :

$$(F_m\,l_m)_{min} = \frac{1}{\eta_m\,P_m}\,\frac{\Phi_n^2}{(HB)_{max}} \qquad .. \qquad .. \qquad (34)$$

The optimum dimensions of the magnet are then fully determined by eqs. (32) and (34).

4. Magnetic Circuit with Constant Flux, and Subsequent Demagnetization Owing to Disturbing Fields Occurring at Irregular Intervals.

In practice it frequently occurs that the magnet must be capable of generating a given constant flux in spite of its having been subjected to considerable de-

* The formulae used for this purpose are given in an appendix to the original paper.

magnetizing influences, which may for instance be due to its own stray field if the magnet has been magnetized separately or with only a part of the magnetic circuit. It will be shown that for optimum utilization of the magnet in this case, both p_n and p_s must assume certain critical values.

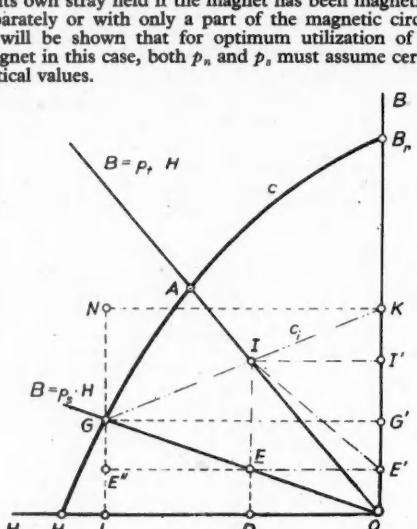

Fig. 5. **Constant flux, with subsequent demagnetization by a disturbing field.**

When the magnet is removed from the magnetizing apparatus after magnetization, its working point changes its position on curve *c* (see Fig. 5) and passes the point *A* at which it would have remained if the magnet had been magnetized after completing the assembly of the magnetic circuit, until it reaches point *G* which is the intersection of curve *c* with the straight line $B = p_s H$ representing the stray field of the magnet. If the magnet is now placed in the arrangement for which it was designed, the point *G* will not move on *c* back to *A* but will come closer to the *B*-axis on an inner demagnetization curve, known as the "recoil line," c_i, and finally reach a point *I* which is the intersection of c_i with the straight line *OA* determined by the total specific permeance p_t. If the curve c_i is described several times (for instance by repeatedly removing and replacing the magnet), then it will be found that c_i is a narrow, nearly closed loop which gradually changes its position until it finally closes itself after a certain number of cycles, when its position also becomes stable. For practical purposes it can be replaced by the straight line *GK* in the second quadrant of the *H*-*B* plane. Its slope relative to the (now negative) *H*-axis is known as the "reversible permeability" μ_{rev}. According to the position of its starting point *G* on curve *c*, μ_{rev} will vary (by approximately 20 per cent for the newest magnetic alloys, and up to 50 per cent for the older types), and the variation is such that starting from point $(H, B) = (H_c, 0)$, μ_{rev} will decrease slowly whilst approaching $(H, B) = (O, B_r)$ without, however, reaching unity.

Besides H_c, B_r, H_0, B_0, and $(HB)_{max} = (H_0\ B_0)$, the mean value of μ_{rev} in the neighbourhood of (H_0, B_0) is a further characteristic quantity which is essential for a correct dimensioning of the magnet.

These considerations show that in nearly all cases where the dimensions of a magnetic circuit have to be determined, it is not advisable to take as working-point the point (H_0, B_0) on the normal demagnetization curve *c*, since under the influence of a disturbing field the magnet leaves this point and does not return to it again. Instead, the magnet which has already been magnetized should be subjected to an external field (for instance to its own stray field), which is at least as great as any disturbing field which may be expected to appear later on.

In general it is recommended to design magnetic circuits which are to be stabilized by an artificial field, in such a way that they may be magnetized when the useful permeance is not yet incorporated in the circuit (for instance, a polarized relay should be magnetized without its armature, a telephone receiver without its diaphragm, and a lifting magnet without its load), so that in order to determine the stabilizing field, which is equal to the field in the magnet after magnetization, only the stray permeance of the circuit will have to be taken into consideration.

Under these conditions, the slope of the straight line *OG* in Fig. 5 will be equal to the specific permeance p_s of the stray fields of the magnetic circuit. After magnetization, the assembly of the system is completed, and as a result *G* will move along c_i up to the point of intersection *I* with the straight line *OA* characterizing the new magnetic equilibrium. The slope of *OA* is therefore equal to the total specific permeance $p_t = p_n + p_s$.

The total mean flux density coming from the magnet is represented by the line $\overline{DI}$, of which $\overline{EI}$ represents the useful flux density, and $\overline{DE}$ the stray flux density. The slope of $E'I$ is again equal to p_s, whilst $\overline{E'E} \cdot \overline{EI}$ represents the useful energy-density W_n.

Optimum utilization of the magnet is achieved if the energy in the air-gap, and hence also W_n, is a maximum. For a given position of *G* this will be the case if $\overline{E'E} = \overline{G'G}/2$; then $\overline{E'I'} = \overline{OK}/2$ and therefore the rectangle $I\,I'\,E'\,E$ inscribed in the triangle *OGK* will have a maximum value, equal to half the area of *OGK*.

The slope μ_{rev} of the inner demagnetization curve c_i, that is, of the straight line *GK* (see Fig. 5), can be obtained as follows :

$$\mu_{rev} = \overline{G'K}/\overline{G'G} = (\overline{OK}-\overline{OG'})/\overline{G'G} =$$
$$= (\overline{OK}/\overline{G'G})-(\overline{OG'}/\overline{OL}) = (\overline{EI}/\overline{EE'})-(\overline{LG}/\overline{OL}).$$

When *I* is at its optimum position, $\overline{EE''} = \overline{E'E}$. Apart from this we always have

$$p_n = \overline{EI}/\overline{E'E} \text{ and } p_s = \overline{LG}/\overline{OL}.$$

so that for the optimum position of *I*, when *G* is given,

$$p_s{}^* = p_n - \mu_{rev} \quad .. \quad .. \quad (35)$$

Thus for any value of the useful permeance p_s, the optimum specific stray permeance, $p_s{}^*$, is given by eq. (35).

Furthermore, in order to determine the optimum position of *G*, the area of the triangle *OGK*, which is equal to $2W_n$, should be as large as possible ; this will be the case for the rectangle *OLNK*, which is twice as large, and the area of which is given by

$$f = H\,[B + \mu_{rev}\,H] \quad .. \quad .. \quad (36)$$

f is a maximum when $df/dH = 0$, i.e. when its variation is zero :

$$df = 0 = d\,[H\,(B + \mu_{rev}\,H)]$$
$$= d\,(HB) + d\,(\mu_{rev}\,H^2),$$

and we obtain as a condition for the optimum position of *G* :

$$df = d\,(HB) + 2\,\mu_{rev}\,HdH = 0 \quad .. \quad (37)$$

regarding μ_{rev} as constant in the first approximation.

Hence the co-ordinates of *G* must satisfy the conditions

$$H_G > H_0,\ B_G < B_0 \quad .. \quad .. \quad (38)$$

since only under these conditions the differential quotient $d(HB)/dH$ will be negative as required by eq. (37).

Substituting eq. (37) in eq. (25) which determines

the demagnetization curve in the second quadrant of the B–H plane (with H replaced by $-H$), we obtain a cubic equation for the abscissa $H_{G\,opt}$ of G_{opt}, and this equation can be solved numerically.

The point G_{opt} can be determined with very good approximation in the following manner : We first plot the curve

$$B_1 = B(H) + \mu_{rev} H$$

in the neighbourhood of point (H_0, B_0) by adding to each ordinate of c the product of its abscissa and the corresponding reversible permeability. By intersecting this curve c_1 (B_1) with the straight line

$$B = \frac{B_r}{H_c} H = \frac{B_0}{H_0} H,$$

a point of intersection N is obtained which has practically the same abscissa as the point G_{opt}, so that the parallel to the B-axis passing through N will intersect the demagnetization curve at the required point G_{opt}.

In brief, it may be said that : (1) if no disturbing fields are subsequently expected to occur, the optimum working point of the magnet is at the position (H_0, B_0) and the total specific permeance $p_t = p_n + p_s$ is thereby determined, it being understood that p_s should be made as small as possible ; (2) if disturbing influences are expected at irregular intervals, then an optimum utilization of the magnet will only be achieved for certain critical values of p_n and p_s. As long as the disturbing field is not greater than $\overline{OQ}$, where QG_{opt} is parallel to OI_{opt} (the disturbing field causes a displacement of the co-ordinates relative to O), the working point of the magnet will go back to its original position I_{opt} after the disturbance has vanished, so that there will be no change in the equilibrium position.

The value of $p_{n\,opt}$ can now be determined from the construction used to find G_{opt} and I_{opt}. From Fig. 6 we find that $\overline{OD} = \overline{DL}$. As ON is a diagonal of the rectangle $OLNK$, we have $\overline{DP} = \overline{OK}/2$. Moreover, for the optimum working point we have

$$\overline{EI}_{opt} = \overline{E'I'}_{opt} = \overline{OK}/2 = \overline{DP},$$

so that finally

$$\overline{EI}_{opt}/\overline{E'E} = \overline{DP}/\overline{OD} = \overline{LN}/\overline{OL} = B_0/H_0 = B_r/H_c.$$

Therefore, when $I = I_{opt}$, the specific useful permeance $p_{n\,opt}$ which is determined by the slope of the straight line $E'I_{opt}$ relative to the H-axis, is given by

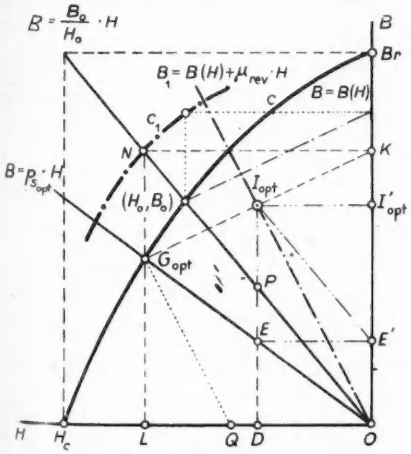

Fig. 6. **Determination of the optimum working point when demagnetization by a disturbing field is expected at irregular intervals.**

$$p_{n\,opt} = B_0/H_0 = B_r/H_c \quad .. \quad .. \quad (39)$$

For the optimum specific permeance of the stray field, $p_{s\,opt}$, this gives, together with eq. (35) :

$$p_{s\,opt} = \frac{B_r}{H_c} - \mu_{rev} \quad .. \quad .. \quad (40)$$

This equation can also be obtained directly from Fig. 6, since

$$\overline{LG}_{opt} = \overline{LN} - \overline{G_{opt}N},$$

and eq. (40) is obtained by dividing both sides of this equation by the abscissa $\overline{OL}$.

With eqs. (27), (29), and (40), the optimum magnetic efficiency $\eta_{m\,opt}$ is then

$$\eta_{m\,opt} = \frac{p_{n\,opt}}{p_{t\,opt}} = \frac{\dfrac{B_r}{H_c}}{2\,\dfrac{B_r}{H_c} - \mu_{rev}}$$

or

$$\eta_{m\,opt} = \frac{1}{2 - \mu_{rev}\dfrac{H_c}{B_r}} \quad .. \quad (41)$$

a value which is somewhat greater than 0·5 or 50 per cent and which in many cases is not achievable in practice.

To avoid laborious computations, the foregoing methods for the dimensioning of magnetic circuits should only be used after making first a rough estimation to find the order of magnitude of the dimensions of the magnet, and this preliminary work can be simplified considerably by using empirical formulae, for instance the formulae evolved by E. Underhill[4].

5. Conclusions.

Various other types of magnetic circuits for which the dimensions can be determined by means of the above methods, are given in Desmond's investigation[2].

When magnets without pole-pieces are used, it is no longer justified to assume that all the lines of flux come out of the front faces of the magnet, and hence that the magnet is homogeneously magnetized. The rotational ellipsoid magnet is the only type of non-bent magnet which has a homogeneous polarization. For an exact calculation of all other types of magnets, particularly when no pole-pieces, or only very small ones, are provided, the useful flux and the leakage or stray flux have to be determined by step-by-step methods, which were first applied by Evershed[3]. For this purpose one assumes that the magnet is subdivided into a number of regions symmetrical relative to its centre, and in each of these H_m and B_m are assumed to have constant values, whilst the leakage flux can only come from the junctions between these regions.

The effect of non-homogeneous magnetization can be illustrated by an example from Desmond's work[2]. Two similar horse-shoe magnets of constant cross-section are placed with their ends touching each other, and are then magnetized. As the circuit thus formed can be regarded as free from leakage, the flux density can be assumed to be constant at every point and equal to the residual magnetization. If the magnets are separated after magnetization, then the working points of the centres and of the ends of the magnets will move to two different positions on the demagnetization curve, with the result that when the two magnets are brought together again the two working points will move back towards the B-axis along two different recoil curves. As the composite circuit was assumed to have no stray

field losses, one might expect the two working points to reach finally the B-axis, and thus satisfy the condition $\oint dsH = 0$. However, the fluxes at the ends and at the centres will then have different values, although this is not possible if the stray losses are equal to zero. To satisfy the conditions of continuity and of an irrotational field, the working point of the ends must therefore move over its corresponding inner demagnetization curve beyond the B-axis, into the first quadrant of the (normal) H-B plane, whilst the working point of the magnet centres remains within the second quadrant.

BIBLIOGRAPHY.

(1) E. WATSON : *J.I.E.E.*, Vol. 61, 1923, *p* 641.
(2) D. DESMOND : *J.I.E.E.*, Vol. 92, 1945, *pp.* 229-252.
(3) S. EVERSHED : *J.I.E.E.*, Vol. 58, 1920, *pp.* 780-837.
(4) E. UNDERHILL : *Electronics*, Dec., 1943, *p.* 126.
(5) A. VAN URK : *Philips Technische Rundschau*, Vol. 5, 1940, *pp.* 29-36.
(6) E. SPAHN: *Schweizer Archiv*, Vol. 10, 1944, *pp.* 313-322.

RUSSIA

The Effect of Shape and Size Factors on the Fatigue Strength

By N. N. APHANASIEV. (From "A Collection of Papers on the Dynamic Strength of Machine Parts," *Institute of Practical Engineering of the Academy of Science, U.S.S.R.*, 1946, pp. 157-167, 11 illustrations.)

IT has been established by numerous investigations that an increase in the dimensions (diameter) of test pieces lowers their fatigue limit, and that this phenomenon becomes more apparent where stress concentrations occur. It is known, however, that the ratio of the fatigue limit of a smooth test piece (i.e. one not subject to stress concentration) to that of a notched piece is usually greater than unity. Hence the fatigue limit of a test piece subject to stress concentrations is usually defined by a nominal stress acting over the root cross-section, and the ratio is known as the effective coefficient of stress concentration, i.e.

$$\beta = \frac{\sigma_{\text{smooth}}}{\sigma_{\text{notched}}} \quad .. \quad .. \quad (1)$$

This effective coefficient of stress concentration does not, in most cases, exceed the theoretical coefficient, α, where

$$\alpha = \frac{\sigma_{\max}}{\sigma_{\text{nom}}} \quad .. \quad .. \quad .. \quad (2)$$

The relation between the effective and theoretical coefficient of concentration depends on the shape and dimensions of the pieces, and the material from which they are made. Usually β approaches the value of α when the absolute dimensions of a piece increase, when the gradient of stress decreases, and when comparatively high-strength materials are used. For small test pieces of some metals, $\beta = 1$ (as in the case of austenitic steels and some types of light alloys).

The deviation of the effective stress concentration factor from the theoretical coefficient is characterized by the notch sensitivity of the metal, η, where

$$\eta = \frac{\beta - 1}{\alpha - 1} \quad .. \quad .. \quad .. \quad (3)$$

or

$$\beta = 1 + \eta(\alpha - 1) \quad .. \quad (3a)$$

Relations of a similar kind were obtained based on a hypothesis that the difference between β and α is due to a lowering of peak stresses owing to plasticity[1]. Fig. 1 is a diagrammatic representation showing how the coefficient η originates.

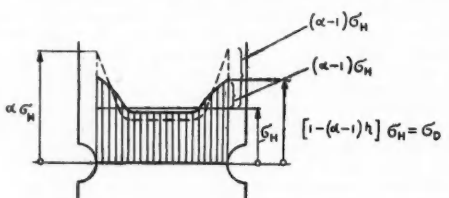

Fig. 1.

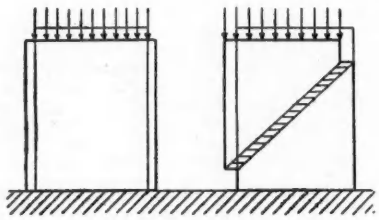

Fig. 2.

The dotted line indicates the stress distribution over the root cross-section of the notched test piece and the full line relates to the same case with lowered peak stresses owing to plasticity. It is thus shown that notch sensitivity is expressed by the degree of lowering of the peak stress, taken as a percentage of the mean stress in the given section.

Investigations[2,3] have shown that the notch sensitivity of a material depends not only on the properties of the material used, but also on the shape and dimensions of the test piece. This peculiarity complicates the estimation of endurance strength. Apart from this, however, no lowering of stress at notches is observed, under varying stresses not exceeding the yield limit. Consequently, according to some workers[4,5,6] this hypothesis is not confirmed by experiment.

Kuntze[7] doubts whether the hypothesis of lowered peak stress corresponds to experimental results and propounds his own theory explaining the non-sensitivity to notching of metals by the mechanism of plastic deformation. According to this author there is not only a slip in the cross-section of the tested piece at plastic deformation, but bending of the fibres also occurs. (See Fig. 2.) In notched specimens offering sufficient resistance to separation, plastic deformation is bound to take place simultaneously throughout the section and stress concentration will not influence the loading at which yielding occurs. Where the cohesive strength is insufficient, sliding occurs in a part of the section only, and the material loosens where there is no slip (Fig. 3). Thus, according to Kuntze,

notch sensitivity of a material is explained by a relatively low cohesive strength.

Dehlinger[8] also contests the hypothesis of the lowering of the peak stresses in points of stress concentration

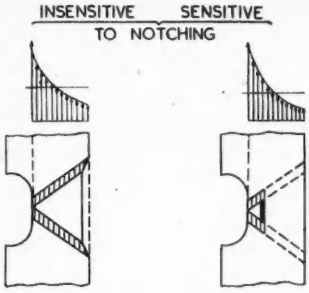

Fig. 3.

and explains the non-sensitivity to notching as a slowing down in the development of fatigue cracks owing to the rapid decrease of stress from the surface towards the centre of the specimen. Against Dehlinger's theory, it is well known that where hair cracks occur, the fatigue limit falls very rapidly[9], and the possible retardation in the development of cracks may influence only the shape of the Woehler curves, but not the fatigue limit.

Attempts were made to connect the fatigue limit of specimens subject to stress concentrations with the stress gradient, and the author derived an empirical relation between fatigue limit and the relative stress gradient in the form[10].

$$\sigma_H = \frac{\sigma_0}{\alpha}\left(\frac{z}{A}+1\right)^b \quad .. \quad .. \quad (4)$$

where σ_H is the nominal stress in a notched specimen, α is the theoretical stress concentration factor, and z is the relative stress gradient equal to the ratio of the stress gradient to the nominal stress in the specimen, whilst A and b are constants for the material. This was obtained by evaluating data given by Faulhaber and Buchman. A shortcoming of the given formula lies in the fact that z, and consequently A, have the dimension 1/mm ; the constant for the material should be dimensionless.

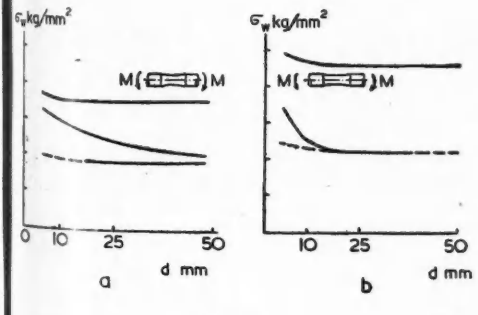

Fig. 4.

Peterson[11] bases his explanation of the size and shape factors on experimental results which show that the fatigue limit of smooth test pieces decreases slightly with increasing dimensions (diameter). In Fig. 4, relating to a nickel-molybdenum steel $\sigma_b = 68$ kg/mm² and a chrome-nickel steel $\sigma_b = 85$ kg/mm², the full lines at the top represent this case, the scale divisions of the ordinate corresponding to 10 kg/mm². If the effective coefficient of stress concentration coincided with the theoretical coefficient, the lower dotted line would give the fatigue limit for notched specimens. Actually, however, the fatigue limit of notched specimens varies according to the middle full line, and as the diameter of the specimen increases, the curve of the actual fatigue limit asymptotically approaches the curve of the theoretical fatigue limit (see Figs. 4a and b). Different materials, having different notch sensitivities, are characterized only by the curve of the actual fatigue limits. But Peterson overlooked that, for different materials, the curves of fatigue limit variations must be different when plotted against the diameter of unnotched specimens.

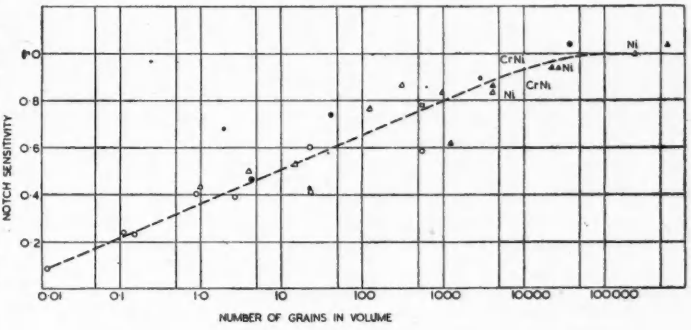

Fig. 5.

Peterson says that the different character of the fatigue limit-curves of notched specimens plotted against diameter depends on the grain size of the metal. In Fig. 5 the ordinate represents the notch sensitivity, η (where $\eta = \frac{\beta-1}{\alpha-1}$) and the abscissa the number of grains in the volume stressed within the limits 0·95 — — 1·00 of the maximum. Thus it is shown that there is a connexion between grain size and notch sensitivity, but it is not a functional relation. It is obvious that apart from the grain size, a number of other metallurgical factors influence the notch sensitivity.

Oding[12] developed the views of other workers (e.g. Föppl's) regarding a relation between notch sensitivity and the area of the hysteresis loop at an amplitude corresponding to the fatigue limit (cyclic viscosity). He also maintains that the grain size is responsible for the dimensional factor.

The author has mentioned in a previous paper[13] that the relation between " cyclic viscosity " and notch sensitivity may be explained from the viewpoint of the statistical theory of fatigue of metals. A weakness of Oding's theory must be seen in that it attempts to explain size factor and notch sensitivity from two different assumptions, whereas experimental data indicates a probability that both are due to the same property of the metal.

Attempts have been made to use an empirical relation for calculating shape and notch factors. Thus, Moor[14] suggested the following formula for specimens having an annular notch

$$r' = k_1 d^{\frac{1}{2}} - k_2 t + r \quad .. \quad .. \quad (5)$$

where r is the fillet radius, t is the depth of the fillet, d is the root diameter of the specimen, k_1 and k_2 are constants, and r' is a fictitious fillet radius which, from Neuber's graph, gives a theoretical stress concentration factor coinciding with the effective factor. Such an empirical formula, however, is very cumbersome and of little practical value.

Recently efforts were made to explain the mechanism of brittleness, and to a certain extent the mechanism of fatigue, by statistical means. Among the most interesting papers in this respect are Weibul's[15] and Kontorova and Frenkel's[16]. Both these papers are unsatisfactory, however, in that they presume some artificial conception of defects in the material (Kontorova and Frenkel). In this abstract form the determination of brittle failure by the statistical theory has no relation to other properties of the material when applied to fatigue problems.

A better solution, while evaluating the known properties of a metal, would be to link them to form a consistent system and from this point of view Orowan's[17] paper is of interest because it describes the process of fatigue, and the computation of a Woehler curve.

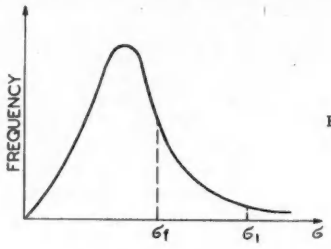

Fig. 6.

The author presented a statistical theory of fatigue[13, 18] based on the assumption that the metal is a conglomerate of grains stressed differently under the effect of external forces, the varying stresses being due to the inhomogeneity of the structure, porosity, slag inclusions, the influence of the grain boundaries, etc. Thus the frequency of the occurrence of any particular stress value acting on an individual grain may be expressed as a function of the stress value (see Fig. 6)

$$Y = f(\sigma) \quad .. \quad .. \quad .. \quad (6)$$

The metal grains are regarded as uniform elements whose characteristics approach those of ideal monocrystals. It is known that the yield limit and, probably, the cohesive strength of individual crystals must be the same for a given crystallographic direction.

To simplify the calculation all grains are assumed to have identical characteristics (i.e. yield limit and cohesive strength) in the direction of the acting force, but are subjected to different stresses according to the individual orientation of the crystal concerned.

Denoting the probability function for the stress of individual grains by $F(z)$, the equation for the statically stressed metal can be given the form[13]

$$\sigma_\epsilon = \sigma_f \left[1 - \frac{1}{z_0} \int_0^{z_0} F(z)\, dz \right] \quad .. \quad (7)$$

Where σ_ϵ is the stress corresponding to an elongation ϵ and σ_f is the yield limit (uniform for all grains)

$$z = \frac{\sigma}{a}\ ;\ z_0 = \frac{\sigma_f}{a}\ ;\ a = \epsilon E$$

Eq. (7) makes no allowance for strain hardening nor for changes in orientation of the crystal due to tensile strain. To introduce a factor allowing for the first mentioned of these phenomena does not entail special difficulties[13, 18], and the second factor need not be considered where small relative extensions in the order of 1–2 per cent are involved.

The experimental tensile test curves may be sufficiently well represented in the form[13]

$$F(z) = \frac{z^k}{A^k + z^k} \quad .. \quad .. \quad .. \quad (8)$$

Consequently, the parameters of the probability function can be found from the tensile test curves of the metal. On the other hand, the probability of the occurrence of fatigue cracks is determined by the presence of grains with a stress component exceeding the cohesive strength[18]. (This stress component is the product of the total relative elongation mentioned and the modulus of elasticity.) For rolled and forged metals having fibrous structure the transition from one cross-sectional layer to another can hardly produce new combinations of stresses acting on the single grains, and the probability of the presence of over-stressed grains may be determined from one cross-section only.

Accordingly, the probability of fatigue cracks occurring will be

$$W = [1 - F(z_T)] \quad .. \quad .. \quad (9)$$

where $z_T = \sigma_T/a$, i.e. z is equal to the quotient of cohesive strength by the stress component, a. The total number of grains in the cross-section being AF, and assuming that the presence of not more than a single grain subject to over-stress (i.e. exceeding the cohesive strength) will produce fatigue failure, the condition for finding the fatigue limit, is :—

$$AFW = 1 \quad .. \quad .. \quad (10)$$

Introducing the probability function of eq. (8), after simplification with respect to second order terms, we get

$$AF\sigma^k = 1 \quad .. \quad .. \quad .. \quad (11)$$

Thus it is possible to determine from tensile tests, the fundamental parameter of the law of variation of the fatigue limit with test conditions.

As an example of the practical application of eq. (11) the following gives the calculation of the influence of the notch form on the fatigue limit of a circular specimen. Of decisive influence on the fatigue limit of a notched specimen (stress concentration) is only the zone in which the maximum stresses in the specimen occur. For this part of the stress curve a parabolic law may be assumed

$$\sigma_x = \sigma_m \left(\frac{x}{r} \right)^p \quad .. \quad .. \quad .. \quad (12)$$

and eq. (11) takes the form

$$A \int_0^r 2\pi x\, dx\, {\sigma_x}^k = 1 \quad .. \quad .. \quad (12a)$$

Hence the following expression for the effective concentration factor is obtained[13]

$$\beta = \frac{\sigma_0}{\sigma_n} = \alpha \sqrt[k]{\frac{k+r}{pk+r}} \left(\frac{r}{r_o} \right)^2 \quad .. \quad .. \quad (13)$$

The maximum gradient of stress for the case of a stress distribution corresponding to eq. (12) is

$$\Delta = \frac{d\sigma_x}{d\sigma_{x=r}} = \frac{\sigma_m p}{r} \quad .. \quad .. \quad .. \quad (14)$$

or

$$p = \frac{\Delta r}{\sigma_m}$$

i.e., p is the relative gradient of the stress. For the sake of combining experimental and theoretical data, a hyperbolic law of stress distribution is assumed, as before, and used in the determination of the maximum stress gradient :

$$\Delta = \frac{\sigma_{max}}{r}\left(1 + \frac{r}{\rho} - \frac{Br}{\rho}\right) \quad .. \quad .. \quad (15)$$

where r is the radius of the specimen at the smallest cross-section, ρ is the radius of the notch, and B is a constant depending on the geometry of the specimen. The relative stress gradient p may be calculated approximately using the equations

for $\rho/r \leqslant 0{\cdot}2$

$$p = \frac{r}{\rho}\left(\frac{\rho}{r} + 0{\cdot}8\right) \quad .. \quad .. \quad (16a)$$

for $\rho/r \geqslant 0{\cdot}3$

$$p = \frac{r}{\rho}\left(\frac{\rho}{r} + 1\right) \quad .. \quad .. \quad .. \quad (16b)$$

From the above considerations, namely that the part of the volume where the maximum stress occurs, has the decisive influence on the fatigue limit, and that in this region the hyperbolic distribution law may be replaced by a parabolic law (with the same value for the maximum relative stress gradient), and to avoid complicating the solution of the problem, the value of the relative gradient found from eqs. (16a) and (16b) was introduced into eq. (13).

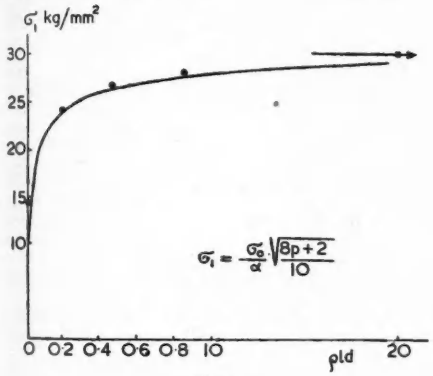

Fig. 7

Fig. 7 represents the curve of the variations of fatigue limits against varying ρ/d, i.e. the ratio of the fillet radius to specimen diameter, the latter being kept constant. The curve is computed from eq. (13) assuming $k = 8$. On the same graph points taken from Lehr and Mailänder's paper[20] are entered for the case of two different diameters with one constant radius. As shown in Fig. 7, agreement between the calculated curve and the experimental results is very satisfactory and, therefore, the theory may be said to describe with sufficient accuracy the influence of the various concentration factors on the fatigue limit.

From experimental evidence it can be concluded that with increasing diameter the decreasing fatigue limit of the specimens tends towards a certain limiting value. Such results can be obtained by using the statistical theory if a curve of frequencies of stress distribution over individual metal grains is assumed to intersect with the axis of the abscissae (Fig. 8). When a frequency curve as shown is assumed, the stress, eq. (7) changes so that, for the initial part of the stress diagram (so long as σ_{max} determined by the frequency curve does not reach the value of the yield limit of the grain) Hooke's law holds good. Obviously the assumption of an absolute elastic limit following from this (namely a finite elastic limit) is not contradicted by experimental facts.

The computation of the probability of a fatigue failure reduces, in this case, to the determination of the shaded area in Fig. 8 (to the right of σ_T). Unfortunately, however, the general solution of this problem for the purpose of determining the effective concentration coefficient presents considerable difficulties.

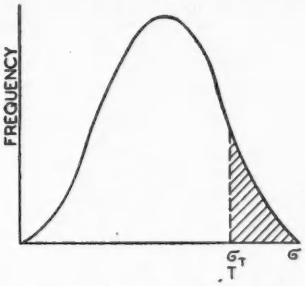

Fig. 8

From an analysis of the equations obtained 1, the following tentative expression for the effective concentration coefficient may be assumed, based on a frequency curve corresponding to that in Fig. 8

$$\beta = \alpha \frac{1 + B\sqrt[k]{\frac{p_1 k + 2}{d_1^2}}}{1 + B\sqrt[k]{\frac{p_2 k + 2}{d_2^2}}} \quad .. \quad .. \quad .. \quad (17)$$

where B and k are constants depending on the material only, p is the relative stress gradient, while d_1 and d_2 are the diameters of the two specimens compared. Eq. (17) is suitable for the case of bending and extension of a circular specimen. If, e.g., the first specimen the fatigue limit of which is to be determined, is smooth, then, in bending, $p = 1$. Let us assume that the diameters of both specimens are equal. The result, according to eq. (17) will then be as follows :— When the diameter of the specimens tends towards infinity then $\beta \to \alpha$. The same result is obtained when either

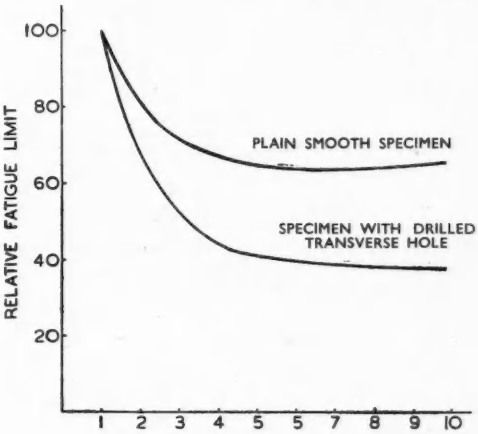

Fig. 9

k tends towards infinity, or B towards zero. On the other hand, it is evident that when the diameter of the second specimen grows infinite (both specimens being smooth) the relation of the fatigue limits for the two specimens will become

$$\beta = 1 + B\sqrt[k]{\frac{k+r}{d^2}} \quad .. \quad .. \quad (17a)$$

Also, it is clear from eq. (17) that if the relative gradient grows, the effective concentration factor will decrease. In Fig. 9, the fatigue limit of two types of test specimens of the same material ($B = 1{\cdot}3$, $k = 5$) is plotted against the logarithm of the diameter, the fatigue limit of specimens of 10 mm diameter being taken as unity for comparison. The graph shows that the fatigue limit of the specimens with drilled transverse holes (stress concentrations) decreases more rapidly than that of plain specimens.

Thus eq. (17) describes very satisfactorily the qualitative curve of the variation of the fatigue limit with the shape and dimensions of the specimen. For the purpose of quantitative evaluation of eq. (17) the results of determinations of the fatigue limits of drilled specimens from Lehr's[20] and Peterson's papers[3] were used. No particular care was taken in the selection of the parameters for eq. (17), as the systematic error in Lehr's and Mailänder's determination of the fatigue limit (carried out on 2-4 specimens) was very considerable.

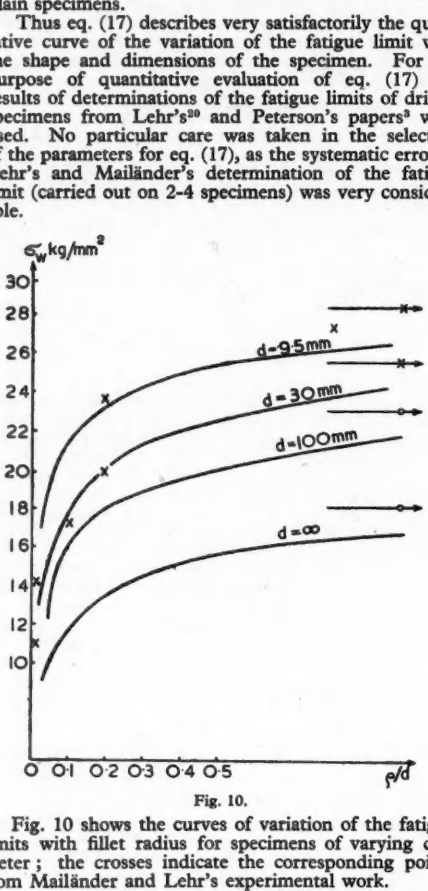

Fig. 10.

Fig. 10 shows the curves of variation of the fatigue limits with fillet radius for specimens of varying diameter; the crosses indicate the corresponding points from Mailänder and Lehr's experimental work.

Eq. (17) in this case takes the following form :

$$\beta = \frac{\sigma_0}{\alpha} \frac{1 + 1{\cdot}3\sqrt[5]{\frac{p_1 + 0{\cdot}4}{d_1^2}}}{1 + 1{\cdot}3\sqrt[5]{\frac{p_2 + 0{\cdot}4}{d_2^2}}} \quad .. \quad (17b)$$

In Fig. 11 the effective concentration factors are plotted against specimen diameter for two ratios of

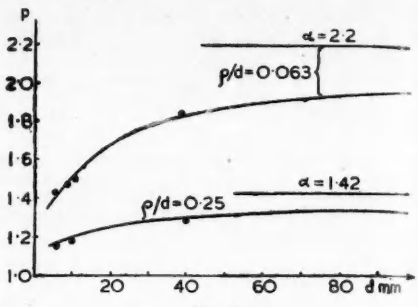

Fig. 11.

fillet radius to the minimum diameter of the specimen. Peterson's experimental results are indicated by points on the same graph. In this case eq. (17) takes the form

$$\beta = \alpha \frac{1 + 2{\cdot}2\sqrt[3]{\frac{1{\cdot}67}{d^2}}}{1 + 2{\cdot}2\sqrt[3]{\frac{p + 0{\cdot}67}{d^2}}} \quad .. \quad (17c)$$

As shown in both figures, the experimental results are satisfactorily represented by eq. (17).

Thus, the theory presented makes it possible to ascertain the properties of a material by a small series of fatigue tests from which further calculations can be carried out in cases where it is possible to determine the stress gradient and the theoretical stress concentration factor. It should be noted that the equation given is suitable for finding the effective stress concentration factor in bending or tensile stressing. Analogous equations applying to other forms of loading could be derived from the same fundamental principles.

The accuracy of eq. (17) must be improved by linking up the constants with the parameters of the probability curve. It will then be possible to derive at least one of the parameters of the equation from the tensile test curve of the metal under investigation.

Greater theoretical precision, where necessary, must be based on corresponding divergencies between theoretical and experimental curves so as not to complicate calculations by factors which might prove of secondary importance.

BIBLIOGRAPHY.

(1) THUM, *Dauerfestigkeit und Konstruktion*, 1932.
(2) HEROLD, *Wechselfestigkeit metallischer Werkstoffe*, 1934.
(3) PETERSON and WAHL, *J. of Appl. Mech.*, No. 1, *p.* A15, 1936.
(4) SCHAAL, *Zs. f. techn. Phys.*, No. 1, *p.* 1, 1940.
(5) GLOECKER, KEMNITZ, SCHALL, *Arch. f. Eisenhüttenw.*, Vol. 13, *p.* 89, 1939.
(6) KEMNITZ, *Zs. f. techn. Phys.*, *p.* 129, 1939.
(7) KUNTZE, *Mitt. Dtsch. Mat.-prüfungsanst.*, Vol. XXXII, *p.* 63, 1937.
(8) DEHLINGER, *Zs. f. techn. Phys.*, Nos. 11, 12, Vol. 115, *p.* 625, 1940.
(9) MAILÄNDER, *Techn. Mitt. Krupp*, Anh. 8-15, 1939.
(10) APHANASIEV, *J. T. Ph.*, No. 8, *p.* 393, 1936.
(11) PETERSON, *Monogr.* "Contributions to the mechanics of solids, dedicated to S. Timoshenko," 1938.
(12) ODING, *Vestnik Metallopromishlennosti*, No. 12, 1938.
(13) APHANASIEV, *J. T. Ph.*, No. 4, *p.* 349, 1941.
(14) MOOR, JORDAN, *J. Appl. Mech.*
(15) WEIBUL. A statistical theory of the strength of materials, *Proceedings*, No. 151.
(16) KONTOROVA, FRENKEL, *J. T. Ph.*, No. 3, *p.* 173, 1941.
(17) OROWAN, *Proc. Roy. Soc.* ser. A, No. 644, *p.* 79.
(18) APHANASIEV, *J. T. Ph.*, No. 19, *p.* 1553, 1940.
(19) APHANASIEV, *J. T. Ph.*, No. 7, *p.* 1153, 1936.
(20) LEHR, MAILÄNDER, *Mitt. Dtsch. Mat.-prüfungsanst.*, Vol. XXVIII, 1936.

CLASSIFIED ABSTRACTS

Numerous important abstracts which, for lack of space, cannot be published in our main editorial columns, are regularly included in condensed form in this section. Subscribers may obtain photostat copies of all original articles at cost.

BRAKES AND CLUTCHES

The Economical Improvement of Railway Brakes.

By T. SHAVGULIDZE. (From *Zheleznodorozhnij Transport, Russia*, No. 1, 1947, pp. 66-68, 4 illustrations.)

THIS article is a contribution to a discussion regarding the replacement of brakes, under the Five-year plan, on 93 per cent of the rolling stock in the Soviet Union by automatic brakes which number 600,000, and represent a gigantic problem. The discussion was opened in 1946, by an article by Prof. Yegorov, who strongly criticised the existing Westinghouse and Matrosov standard types.

The elements of existing brakes which have been criticised are the three valves in the Westinghouse type and the air distributor of the Matrosov brake. Also electro-pneumatic brakes have proved unsuitable, but the introduction of cable-pneumatic accelerators was very promising, because they made it possible to raise the speed of propagation of the brake-wave from the present low value of 230 to 250 m/sec. to 700 to 1000 m/sec. This shortens the braking distance, and allows for the use of simpler distributors. Whilst the air distributor plays an important part by regulating the pressure in the brake cylinder and reservoir, other, not less important, elements of the system should not be forgotten.

Automatic brakes, whatever their system of operation, must rely on an uninterrupted supply of compressed air, and to cover this requirement, there is a steam-air pump on every train. Its uninterrupted and reliable operation depends on the steam-distributing mechanism. All existing steam distributing mechanisms, whether their steam-distribution is positive, semi-positive, or steam-controlled, are unreliable and suffer from frequent breakdowns due to the length and frailty of the control rod for the slide. The slide valve consists of rings up to 32 mm. in diameter, and these are liable to frequent breakage. On the opening of these rings depends continuous working of the pumps, and this demands ample lubrication. The single-valve type of steam distributor possesses only the base slide which is moved from side to side by steam pressure alone. This type is of great interest and is generally more favourable in operation, because it does not require artificial steam cushions to stop the slide in its extreme positions. It is the most economical device of its kind, owing to the absence of two-way valves with their long steam ducts. The first successful and simple design of a single-valve steam distributor for steam pumps is due to Soviet inventors and has fully accredited itself in service tests, which lasted a year. The steam distributors of the existing tandem-pumps were also remodelled to work on the single-valve principle, and were successful. A new type of steam-air tandem-pump with a steam-operated single-valve distributor is being developed, and this will work much more efficiently and economically owing to the absence of a two-way valve with labyrinth seal, and will be suitable for operation with superheated instead of saturated steam.

The most important task in connexion with the Five-Year plan is the design of a universal driver's controller and a smoothly working universal locomotive brake. The universal controller of the author's design, Fig. 1, served well in the final tests on passenger and goods train engines. It is intended for both types

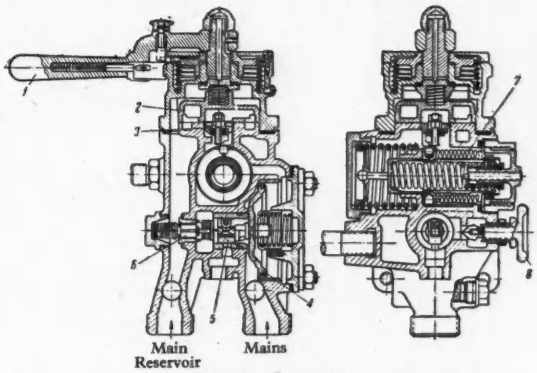

Fig. 1. Driver's Universal Controller.
(1) Handle; (2) Big slide valve; (3) Small slide valve; (4) Piston; (5) Mains valve; (6) Feed valve; (7) Bellows; (8) Adjusting screw.

of engines, and does not require the driver to judge the timing of his controls. Its combination with alarm or accident signals connected to the stop valve facilitates the brake control.

The author has also developed a device which makes communications between the driver and the guard of a train possible for the avoidance of accidents, and to avoid the unintentional locking of wheels, he proposes new types of double-action pump governors incorporating a single air valve. For future development he mentions stream-lined separately activated, tail valves, and states that the introduction of the equipments proposed, will obtain safer conditions and allow for increased traffic on railways.

ELECTROLYTIC POLISHING

The Physico-chemical Behaviour of Oxide-free, Electro-polished Metal Surfaces.

By P. LACOMBE, P. MORIZE and G. CHAUDRON. (From *Revue de Métallurgie, France*, Vol. 44, No. 3/4, March/April, 1947, pp. 87-90, 7 illustrations.)

BY careful control of the electrolytic polishing process, metal surfaces with practically no oxide skin can be obtained. Presence of thin oxide skins can best be discovered by measurement of the dissolution potential of the metal part against a *KCl*—saturated standard electrode in a bath containing 3 per cent *NaCl*. The dissolution potential is e.g. — 1·20 volts for an oxide-free *Al* surface and increases, proportionally with the oxide skin thickness, to — 0·74 volts for *Al* surfaces extensively exposed to air. Measurements at room temperature corroborate Mott's hypothesis that oxide skin thickness increases logarithmically with time. Contact with humidity greatly accelerates the initial skin formation and oxide free polished specimens must be rinsed in acetone and alcohol. The dissolution potential of *Zn* varies from — 1·08 for oxide-free surfaces, to — 0·70 volts after 250 hours exposure to air, and that of iron from — 0·65 to — 0·20 volts. Iron requires very strict control over polishing conditions as contact with humidity leads to instantaneous uniform hydroxide skin formation.

(*Continued on page* 104)

When planning your peace-time production leave the Strip Steel problems to us—

STRIP STEEL for all purposes

HABERSHON

ROTHERHAM

VERSATILITY

AN ALL-PURPOSE SPOT WELDER

PEDAL OPERATED

TYPE E.1504

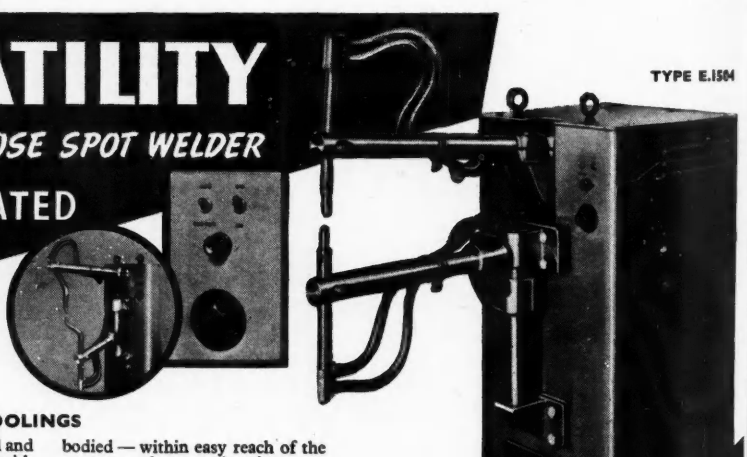

1. UNIVERSAL ARM ADJUSTMENT
2. BUILT-IN TIMER
3. FULL RANGE OF TOOLINGS

Arm movement is both vertical and horizontal — a big advantage with many welding jobs. An automatic welding-time control unit is embodied — within easy reach of the operator. A comprehensive range of toolings is provided for use with this versatile machine.

Send for (a) brochure ED.937 giving a full description of the type E.1504 and its uses, and (b) an illustrated catalogue of all standard toolings.

PHILIPS

RESISTANCE WELDING EQUIPMENT FROM

PHILIPS ELECTRICAL LIMITED

INDUSTRIAL DEPT., CENTURY HOUSE, SHAFTESBURY AVE., LONDON, W.C.2

NEWS OF THE MONTH

Announcements in this section include News relating to British Firms, and on Equipment produced by British Manufacturers.
Available literature may be secured by addressing a request to the advertising department of "The Engineers' Digest," or by writing direct to the manufacturer and mentioning "The Engineers' Digest" as a source.

- PERSONAL
- NEW EQUIPMENT
- BOOKS AND CATALOGUES
- BUSINESS CHANGES
- NOTES

PERSONAL.

Major F. Bentley, M.B.E., has been appointed acting manager of the Manchester branch office of the Atlas Disel Company, Limited, Beresford Avenue, Wembley, Middlesex. The branch is in City Road, Gaythorn, Manchester, and will deal mainly with the compressed-air products of the company.

The Export Promotion Department of the Board of Trade announces the appointment of **Mr. W. H. Young** as deputy director of the British Industries Fair.

Mr. R. Ferguson, M.I.Mech.E., has been appointed consultant director to F. Perkins, Ltd. **Mr. A. Griffiths** has been appointed a director and general manager of the company.

Mr. Henry Hoad, M.I.Mech.E., has relinquished his appointment as Chief Controller, Mechanical Engineering Branch, Control Commission for Germany, and has taken up the appointment of Diesel Contracts manager with Messrs. Davey, Paxman and Company, Limited, Colchester.

Mr. W. Howes has succeeded **Mr. C. Green** as President of the Diesel Engine Users Association.

Mr. Hugh R. Neilson and **Mr. Iain M. Stewart** have joined the board of directors of Messrs. Glenfield and Kennedy, Limited, Kilmarnock, Ayrshire.

Mr. J. G. Robb, deputy engineer-in-chief and chief of the research laboratories of Marconi's Wireless Telegraph Company, Limited, Marconi House, Chelmsford, Essex, has been appointed chief of a new Engineering Division in connection with associated companies. He is succeeded as chief of the research laboratories by **Mr. R. J. Kemp,** who was Mr. Robb's chief assistant.

Mr. W. Symes, M.I.P.E., who, since 1944, has been works' manager of the main works at Trafford Park, Manchester, and the various dispersal factories of Metropolitan-Vickers Electrical Company, Limited, and **Mr. W. A. Coates, M.I.E.E.,** who has been manager of the home sales department of the firm since 1946, have both been appointed to the board of the company.

Mr. J. W. Thomas, B.Sc., LL.B., M.I.E.E., who has been secretary of the British Engineers' Association for the past three years, has been appointed chief education and training officer, British Electricity Authority, Portland Court, 170A, Great Portland Street, London, W.1.

Mr. Joseph Walton, an Assistant Managing Director of Thos. W. Ward Ltd., Albion Works, Sheffield, has been appointed Chairman and Managing Director of the Darlington Railway Plant & Foundry Co., Ltd., and **Mr. Phillip T. Ward** has been appointed a Director of the Darlington Company.

Dr. R. C. G. Williams, M.I.E.E., M.I.Mech.E., has been appointed chief engineer of Philips Electrical Limited, Century House, Shaftesbury Avenue, London, W.C.2, and will advise the Managing Director on all technical matters.

BUSINESS NOTES.

The Richard Crittall Group has formed a separate company named Richard Crittall Marine, Ltd., to deal with marine installations.

The Aluminium Plant and Vessel Company, Ltd., announces that the necessary sanction is being obtained to change its formal title to The A.P.V. Company, Ltd.

E. H. Jones (Machine Tools), Ltd., announces that it has established a research department in its export division, under the control of Mr. C. F. Brook. The company is also setting up an automatics technical department under the direction of Mr. T. J. Corcoran.

The Northern Aluminium Company, Ltd., states that its Birmingham sales office has been moved to 14, Temple Street, Birmingham, 2 (telephone : Midland 5236 ; telegrams : "Noralumin, Birmingham"), and that its south-western area sales office is now at 18, St. Augustine Parade, City Centre, Bristol, 1 (telephone : Bristol 20351 ; telegrams : "Noraluco, Bristol").

The well-known Instrument Companies, **E. R. Watts & Son Ltd.** and **Adam Hilger Ltd.,** are being formed into one Company registered as **Hilger & Watts Ltd.** Hilger & Watts Ltd. will employ 1,300 people in the six existing factories. A new factory in the Greater London area has been planned and approved. A high proportion of the products of Hilger & Watts Ltd. are for export, and the overseas sales will be mainly through Scientific Exports (Great Britain), Ltd. (SCIEX) and, for Engineers' Measuring Instruments, British Engineers' Small Tools and Equipment Co., Ltd. (BESTEC).

THE GAUGE AND TOOL MAKERS' ASSOCIATION.

A Party of 17 Members of the Gauge & Tool Makers' Association, accompanied by the Association Secretary, Mr. Gilbert T. Beach, is visiting the United States of America and Canada next month. The objects of the visit may be broadly summarised as follows :

(a) To confirm arrangements for the export to the U.S.A. and Canada of British precision tools and gauges.

(b) To attend the Exposition and Convention in Cleveland, Ohio, of the American Society of Tool Engineers.

(c) To visit precision gauge and tool making establishments in New York, Cleveland, Cincinnati, Hartford, Chicago, Detroit, Toronto, Ottawa, and Montreal, etc., with a view to studying American and Canadian methods of production and confirming that British tools and prices are competitive with those of the American and Canadian gauge and tool industries.

The American Society of Tool Engineers and the American National Tool & Die Association have arranged extensive visits for the G.T.M.A. Party to gauge and tool-making establishments in the U.S.A., and the Canadian Authorities have prepared for similar facilities to be available in the cities to be visited in Canada.

FOR PROTECTIVE AND DECORATIVE PURPOSES
To resist wear or corrosion as part of the process specification for new parts.

FOR BUILDING UP WORN PARTS
to size and providing resistance to wear and corrosion.

FOR SALVAGING MACHINE SHOP ERRORS
Approved by A.I.D., C.I.A., C.I.E.M.E., etc.
Capacity available—write for particulars.

BRAILEY ELECTROPLATERS LTD.
CHAPEL ST · SALFORD 3 · M/C

B27

PACING PROGRESS

Mirror to truth

James Howell's words—"the face is oftentimes a true index of the heart"—apply as closely to Kearns surfacing and boring machines as to the subject of his thought, even though they were written three centuries ago. Absolute identification of designers' knowledge with users' needs (gained through 40 years' practice and sustained personal contact in the field) results in the production of surfaces and many other finishes of a truth which accurately mirrors that of the machines themselves . . . truly an index to the heart of the matter.

KEARNS FOR BORERS

H. W. KEARNS & COMPANY LTD.
BROADHEATH *near* MANCHESTER
Hopwood

THE PROFESSIONAL ENGINEERS APPOINTMENTS BUREAU.

During 1947 the average number of engineers on the Register was 634, 127 of these being primarily Civil, 260 Mechanical and 247 Electrical Engineers. The number of registered engineers has thus been approximately two-thirds of the total for 1946 when the average was 964. A satisfactory number of vacancies has again been notified by employers, the total for the year being 1048.

The number of offers made to engineers as the result of the Bureau's introductions greatly exceeded the number of actual acceptances and the housing situation must be recognised as the most serious obstacle in the filling of vacancies.

Since it commenced to operate, the Bureau has succeeded in filling some 50 posts overseas, but although a number of engineers on the Register are anxious to emigrate to the Dominions, the Bureau has had difficulty in finding candidates to put forward for posts in the Tropics, which represent a high proportion of the overseas vacancies notified.

Applications for registration for employment are invited from members who belong to the Institution of Civil Engineers, the Institution of Mechanical Engineers, or the Institution of Electrical Engineers, or persons whose engineering qualifications for election or admission to one of those Bodies have been approved by the respective Councils. Employers of Professional Engineers are invited to submit details of positions vacant on their staff, indicating any special requirements and stating the salary range offered.

THE WORK OF THE WELDING RESEARCH TEAM AT THE UNIVERSITY OF BIRMINGHAM, JULY, 1944, TO JANUARY, 1947.

Research Report No. 1 has been published by The Aluminium Development Association giving a description of the lines along which the work has proceeded followed by a diagrammatic analysis of the research programme. Summaries are given of ten separate investigations the results of which have established a good foundation of experimental facts, and indicated a theoretical method of approach that may be of the greatest value in solving the problem of the hot shortness and welding characteristics of aluminium alloys.

The summaries are followed by a note on work by other investigators arising from the findings of the Birmingham team. The publication concludes with general comments and some indications of the possible lines of future investigation.

BOOKS RECEIVED.

Magnesium Fabrications. By L. B. Harkins. Publishers: Pitman Publishing Corporation, New York, Chicago, and Sir Isaac Pitman and Sons Ltd., London. 1st Edition, 1947. 149 pp., 51 figures, 32 tables. 20s. net.

This handbook, the latest in the series relating to "Industrial Materials and Processes," is compiled primarily for the student and the man on the job. However, it gives a valuable background of information regarding established procedures and should enable the modern designer to utilize the useful properties of magnesium and make allowance for its weaknesses.

Although magnesium alloys and aluminium alloys have some similar characteristics, a craftsman trained on aluminium must learn the techniques peculiar to magnesium before he can be fully competent to put it to use. The book has been written to explain these techniques and deals with the production of wrought materials, including sheet, extrusions, tubing and the machining of castings but does not include magnesium foundry technology.

It suits its purpose admirably, is well illustrated, and gives useful technical data in tabulated form.

Classified Advertisements.

The Rate for all classified advertisements is 6d. per word; in bold print 9d. per word; minimum order 6s. Box number advertisements 1s. extra. Instructions together with remittance must be received not later than the 3rd of each month for advertisements to appear in the same month's issue.

MACHINERY, ETC., FOR SALE

NISSEN TYPE HUTS, Ex-Government Stock, 36 ft. by 16 ft., £70 and £80; 24 ft. by 16 ft., £56 and £45. Other Buildings also available. Write for details.—Box, E.D., **Universal Supplies (Belvedere) Ltd.,** 45 Pickford Lane, Bexleyheath, Kent. Telephone: Bexleyheath 4227. Yard and Depot: Crabtree Manorway, Belvedere, Kent.

To the Advertisement Manager, "THE ENGINEERS' DIGEST," 120, WIGMORE STREET, LONDON, W.1.

Please insert the enclosed Classified Advertisement in your next available issue.

Cheque/Postal Order value.....for.....words enclosed

Name .....

Address.. .....

Electrolytic Polishing—*continued.*

Unoxidized *Al* surfaces immersed in a concentrated solution of hydrochloric acid corrode immediately, surfaces exposed to air and covered with an oxide skin remain passive for a certain "induction" period depending on the time of exposure and therefore on skin thickness. Corrosion only takes place after the skin has been broken. Weaker reagents produce similar reactions. Zinc exposed to air, then immersed in water shows slow localized corrosion where the protecting oxide skin had been weak. Zinc immersed immediately after electro-polishing is at once covered by a uniform hydroxide layer. This layer, though insoluble, is not adherent, and corrosion continues under it. After a few hours, corrosion patterns of hexagonal shape can then be seen with an orientation corresponding to that of the metallic crystal.

Generally, the passivity of electrolytically polished materials, as observed by some scientists, must be attributed to invisible oxide or salt skins caused by the special conditions of electro-polishing adopted in investigations. A perfect electro-polish should result in a skinless metallic surface of high chemical reactivity. The measurement of dissolution potential thus leads to the distinction of two classes of electro-polishes, those forming oxide or salt skins on the metallic surface and those producing oxide-free surfaces, a distinction of importance for the theory of complex salts in electro-polishing. It is unlikely that any specific recipe for electrolytic baths can guarantee oxide-free surfaces on all materials. Requirements are too varied. It seems logical, however, to assume that the stability of the anion $Cl\ O^{4-}$ helps to secure oxide-free surfaces by preventing secondary oxidation reactions.

WAD REGD.

FORGING or CLIPPING PRESSES

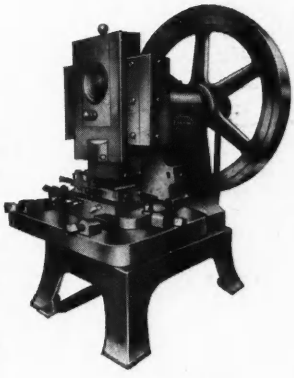

Specially adapted for heavy work in cutting-out, forging, punching, and shearing operations. From 25 to 85 tons pressure.

WALTERS & DOBSON LIMITED
DEPT. E.D.—BAILEY STREET
SHEFFIELD, 1. ENGLAND

ELECTRIC PULLEY BLOCK HOISTS

MATTERSON HOISTS are compact and efficient, require but little attention to keep them in good condition, and are made throughout by men taking a pride in their job. They will not let you down.

Two-speed Hoists with instantly obtainable creeping speed are available, as illustrated.

MATTERSON LIMITED
SHAWCLOUGH TELEPHONE: 4194 ROCHDALE

We proudly announce

The "RAPIER" 1c.c.
DIESEL ENGINE
FOR
VERTICAL OR INVERTED RUNNING

Weight 4 ozs. 7,000 RPM with 10" Airscrew. Will Power Model Aircraft up to 5 ft. span, also suitable for Model Race Cars and :: :: Speed Boats. :: ::

NOT A TOY, BUT A MASTERPIECE OF PRECISION ENGINEERING.

£4 19s. 6d. complete.
Delivery Approximately 4 to 6 Weeks.

The WARWICK LIGHT ENGINEERING
1 LYON STREET, PIN MILL BROW, ARDWICK, MANCHESTER.

"SENIOR"

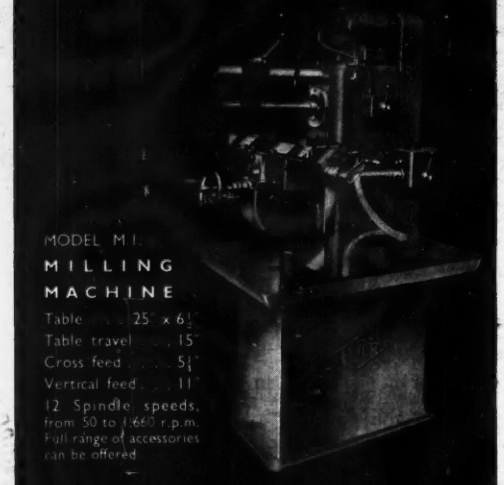

MODEL M.1.
MILLING
MACHINE

Table . . . 25" x 6½"
Table travel . . . 15"
Cross feed . . . 5½"
Vertical feed . . . 11"
12 Spindle speeds, from 50 to 1,660 r.p.m.
Full range of accessories can be offered

For full particulars write to the manufacturers :—

T. SENIOR ATLAS WORKS LIVERSEDGE, YORKS, ENGLAND

PRECISION MACHINING in Repetition Quantities for All Classes of Light Engineering

We can offer the facilities of a well equipped Modern Engineering Plant comprising :—

- AUTOMATIC MACHINES
- CAPSTAN AND CENTRE LATHES
- GRINDING MACHINES, ETC.
- CASE HARDENING AND HEAT TREATMENT
- PRECISION THREAD ROLLING IN ANY METAL

and which is at your service for the production of high class quality components with accuracy and finish.

A.I.D. approved.

The . . .

HANWELL ENGINEERING COMPANY LIMITED

Established 1925 — COUNTESS ROAD NORTHAMPTON — Phone: 3766-3767

S. JELLYMAN, LTD.

Est. 1861

- PLANT ENGINEERS
- FABRICATED STEEL WORK
- TUBULAR STRUCTURES
- WELDING
- MACHINING
- GREY IRON CASTINGS

Cannock Foundry & Engineering Works
CANNOCK, STAFFS.
'Phone : Cannock 2188

ACACIA RD. BOURNVILLE B'HAM 30 ENGLAND

A. F. Exton LTD.

TELEPHONE SELLY OAK 0567

GENERAL ENGINEERS

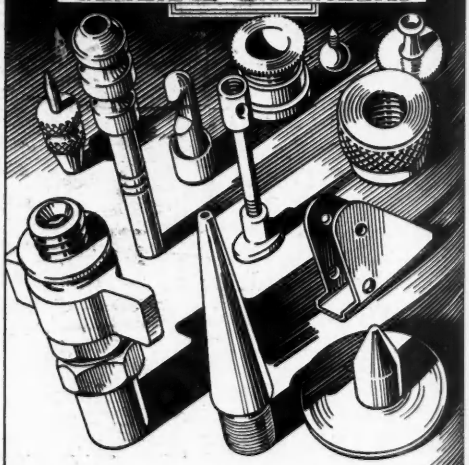

★ Repetition Machining. Pressings. Rivets. Sheet Metal Fabrications. Jigs. Tools. Gauges. Moulds. Press Tools. Cutting Tools, etc., etc.